Published April 8, 2013

Ablation of the mTORC2 component rictor in brain or Purkinje cells affects size and neuron morphology

Venus Thomanetz,[1] Nico Angliker,[1] Dimitri Cloëtta,[1] Regula M. Lustenberger,[1] Manuel Schweighauser,[1] Filippo Oliveri,[1] Noboru Suzuki,[2] and Markus A. Rüegg[1]

[1]Biozentrum, University of Basel, CH-4056 Basel, Switzerland
[2]Department of Animal Genomics, Functional Genomics Institute, Mie University Life Science Research Center, 2-174 Edobashi, Tsu, Mie 514-8507, Japan

The mammalian target of rapamycin (mTOR) assembles into two distinct multi-protein complexes called mTORC1 and mTORC2. Whereas mTORC1 is known to regulate cell and organismal growth, the role of mTORC2 is less understood. We describe two mouse lines that are devoid of the mTORC2 component rictor in the entire central nervous system or in Purkinje cells. In both lines neurons were smaller and their morphology and function were strongly affected. The phenotypes were accompanied by loss of activation of Akt, PKC, and SGK1 without effects on mTORC1 activity. The striking decrease in the activation and expression of several PKC isoforms, the subsequent loss of activation of GAP-43 and MARCKS, and the established role of PKCs in spinocerebellar ataxia and in shaping the actin cytoskeleton strongly suggest that the morphological deficits observed in rictor-deficient neurons are mediated by PKCs. Together our experiments show that mTORC2 has a particularly important role in the brain and that it affects size, morphology, and function of neurons.

Introduction

Mammalian target of rapamycin (mTOR) is a highly conserved serine/threonine protein kinase that controls cell and organismal growth induced by growth factors and nutrients (Wullschleger et al., 2006; Laplante and Sabatini, 2012). mTOR assembles into two distinct, multi-protein complexes, called mTOR complex 1 (mTORC1) and mTORC2, which can be distinguished by their associated proteins and their sensitivity to inhibition by the immunosuppressive drug rapamycin. Whereas rapamycin inhibits mTORC1 acutely, mTORC2 is not inhibited. However, more recent data indicate that prolonged treatment with rapamycin also inhibits mTORC2 (Sarbassov et al., 2006). Thus, some of the effects observed by the application of rapamycin might be mediated by mTORC2. Indeed, insulin resistance in patients that undergo long-term treatment with rapamycin (Cole et al., 2008) has recently been shown to be likely due to inhibition of mTORC2 and not of mTORC1 (Lamming et al., 2012). Thus, the only possibility to clearly distinguish between the function of mTORC1 and mTORC2 in vivo is the generation of mice that selectively lack components that are essential for the function of either mTORC1 or mTORC2.

One of the essential and unique components of mTORC1 is the protein raptor (regulatory associated protein of mTOR; Kim et al., 2002), whereas the protein rictor (rapamycin-insensitive companion of mTOR) is essential and unique for mTORC2 (Jacinto et al., 2004; Sarbassov et al., 2004). Several lines of evidence indicate that mTORC1 is mainly responsible for cell growth and proliferation in response to growth factors, nutrients, or stress, and the two main downstream targets of mTORC1, p70S6 kinase (S6K) and elongation factor 4E binding protein (4E-BP), are key regulators of cap-dependent protein translation (Wullschleger et al., 2006; Laplante and Sabatini, 2012). In contrast, the function of mTORC2 is much less well defined, but experiments in yeast and in cultured mammalian cells have indicated a role of mTORC2 in the regulation of the actin cytoskeleton (Loewith et al., 2002; Jacinto et al., 2004; Sarbassov et al., 2004). mTORC2 also controls phosphorylation of the hydrophobic motif of Akt/protein kinase B (Akt/PKB), protein

V. Thomanetz and N. Angliker contributed equally to this paper.

Correspondence to Markus A. Rüegg: markus-a.ruegg@unibas.ch

Abbreviations used in this paper: CNS, central nervous system; DIV, day in vitro; GAP43, growth-associated protein 43; GSK3, glycogen synthase kinase 3; MARCKS, myristoylated alanine-rich protein kinase C substrate; mEPSC, miniature excitatory postsynaptic current; mIPSC, miniature inhibitory postsynaptic current; mTOR, mammalian target of rapamycin; mTORC, mTOR complex; PKB, protein kinase B; RibKO, rictor brain knockout; rictor, rapamycin-insensitive companion of TOR; RiPuKO, rictor Purkinje cell knockout; SGK, serum- and glucocorticoid-induced kinase; vGLUT, vesicular glutamate transporter.

Supplemental Material can be found at:
http://jcb.rupress.org/content/suppl/2013/04/05/jcb.201205030.DC1.html

The Rockefeller University Press $30.00
J. Cell Biol. Vol. 201 No. 2 293–308
www.jcb.org/cgi/doi/10.1083/jcb.201205030

Published April 8, 2013

kinase C (PKC), and the serum- and glucocorticoid-induced kinase 1 (SGK1), which are all members of the AGC kinase family (Sarbassov et al., 2005; Facchinetti et al., 2008; García-Martínez and Alessi, 2008; Ikenoue et al., 2008).

Germline deletion of *rictor* in mice causes embryonic death (Guertin et al., 2006; Shiota et al., 2006), whereas tissue-specific deletion of *rictor* often results in only minor phenotypes. This is the case in skeletal muscle (Bentzinger et al., 2008; Kumar et al., 2008), adipose tissue (Cybulski et al., 2009), or kidney (Gödel et al., 2011). Importantly, in none of those conditional knockout mice have changes in the actin organization been observed. The rather weak phenotypes caused by *rictor* deletion are in stark contrast to the severe phenotypes observed upon deletion of *rptor* (gene encoding raptor) in the same tissues (Bentzinger et al., 2008; Polak et al., 2008; Gödel et al., 2011). Interestingly, double knockout of both *rptor* and *rictor* aggravate the phenotypes in kidney (Gödel et al., 2011) but not in skeletal muscle (Bentzinger et al., 2008). Moreover, skeletal muscle–specific deletion of *mTOR* largely resembles the phenotype of mice lacking raptor (Risson et al., 2009). These results therefore indicate that most of the known functions of mTOR in several tissues are carried by mTORC1 and that there are significant differences in the importance of mTORC1 and mTORC2 between tissues.

In the nervous system, mTOR has mainly been implicated in protein synthesis–dependent control of synaptic plasticity in learning and memory (Richter and Klann, 2009). More recently, mTOR has been suggested to be deregulated in developmental brain disorders and in neurodegenerative diseases (Crino, 2011). Interestingly, tuberous sclerosis (TSC) patients who suffer from a benign brain tumor caused by mutations in *TSC1* or *TSC2*, which encode proteins that form the main upstream inhibitor complex of mTORC1, frequently also show autism spectrum disorder-like symptoms (Ehninger and Silva, 2011). Thus, the evidence is strong that mTOR signaling is also important in the nervous system. The finding that deletion of the two mTORC1 downstream targets *S6K* or *4E-BP*, and that treatment of mice or rats with rapamycin also affects learning and memory, has resulted in the concept that mTOR in the brain mainly acts via mTORC1 and not mTORC2. Only very recent work has suggested roles of mTORC2 in the regulation of dopaminergic neurons in the adult brain (Siuta et al., 2010; Mazei-Robison et al., 2011). Both of those reports base their findings on the known role of Akt in schizophrenia and morphine-induced addiction, respectively. As mTORC2 has been shown to induce phosphorylation of Akt at Ser473 (Sarbassov et al., 2005), loss of mTORC2 may thus affect the Akt pathway in dopaminergic neurons. Although these conclusions are reasonable, deletion of *rictor* in other species and in other tissues has not revealed strong phenotypes that are based on diminished Akt signaling (Hietakangas and Cohen, 2007; Bentzinger et al., 2008; Cybulski et al., 2009; Gödel et al., 2011). In addition, phosphorylation of Akt at Ser473 is still high in mice deficient for mTOR in skeletal muscle (Risson et al., 2009), indicating that mTORC2 is not essential for the phosphorylation of Akt at Ser473.

We now report on the phenotype of two distinct mouse models where *rictor* was conditionally deleted either in the entire developing central nervous system (CNS) or selectively in cerebellar Purkinje cells, the cell type with highest rictor expression in the brain (Shiota et al., 2006). We show that deletion of *rictor* in the entire CNS causes a strong phenotype that includes severe microcephaly starting at birth and impairment of motor function. Rictor-deficient neurons are smaller and have altered neurite organization. Both the changes in neuron size and neurite morphology are also observed in mice lacking rictor solely in Purkinje cells. Importantly, the morphological changes correlate with the substantial loss of several PKC isoforms and the decrease in phosphorylation of PKC-downstream targets growth-associated protein-43 (GAP-43) and myristoylated alanine-rich protein kinase C substrate (MARCKS), and they are in agreement with the established role of PKCγ in the morphology of Purkinje cell neurons. In addition, mutations in PKCγ cause spinocerebellar ataxia (Chen et al., 2003; Seki et al., 2011), which resembles the motor phenotype of our knockout mice. Thus, our work shows that mTORC2 plays an important role in the brain and that its function in Purkinje cells is cell autonomous.

Results

Germline deletion of *rictor* in mice causes growth arrest and subsequent death between embryonic day 10.5 and 11.5 (Guertin et al., 2006; Shiota et al., 2006). Rictor mRNA is expressed ubiquitously with highest expression in neurons of the adult hippocampus and cerebellum (Shiota et al., 2006; Lein et al., 2007). To circumvent embryonic lethality and to study the role of rictor in the brain, we set out to conditionally delete *rictor* using the Cre/loxP system (Fig.1 A). To do this, we crossed mice homozygous for the *rictor* alleles, in which exons 4 and 5 are flanked by loxP sites (Bentzinger et al., 2008), with mice expressing Cre under the control of the CNS-specific nestin promoter and enhancer (Tronche et al., 1999). This Cre mouse has been shown to induce recombination in all neural tube–derived cells around embryonic day 10.5 (Graus-Porta et al., 2001). After several crosses, we eventually obtained mice that were homozygous for the floxed *rictor* alleles and expressed nestin-Cre (abbreviated herein RibKO [for rictor brain knockout] mice). As controls, littermates were used that either did not express nestin-Cre (and carried the floxed *rictor* alleles) or that were Cre-positive but carried only one targeted *rictor* allele. Successful recombination of the floxed alleles was tested by PCR using primers P1 and P2 (Fig. 1 A) and a nestin-Cre–specific primer set. In genomic DNA isolated from brain, successful recombination was detected in RibKO mice and in mice heterozygous for the floxed *rictor* allele and positive for nestin-Cre (Fig. 1 A). In contrast, no recombination was seen in control littermates that did not express Cre. These data show that our strategy indeed led to the deletion of exon 4 and 5 in the *rictor* gene. This deletion introduces a frameshift and causes a premature stop of translation.

RibKO mice were born in a Mendelian ratio and could not be distinguished from their littermate controls at birth (unpublished data). After a few weeks, RibKO mice developed a rather strong motor phenotype that included a waddling gait (unpublished data), hindlimb clasping upon tail suspension (Fig. 1 B), and a decreased latency to fall off an accelerating rotarod (Fig. 1 C). The brains of RibKO mice were smaller (Fig. 1 D) and weighed

Published April 8, 2013

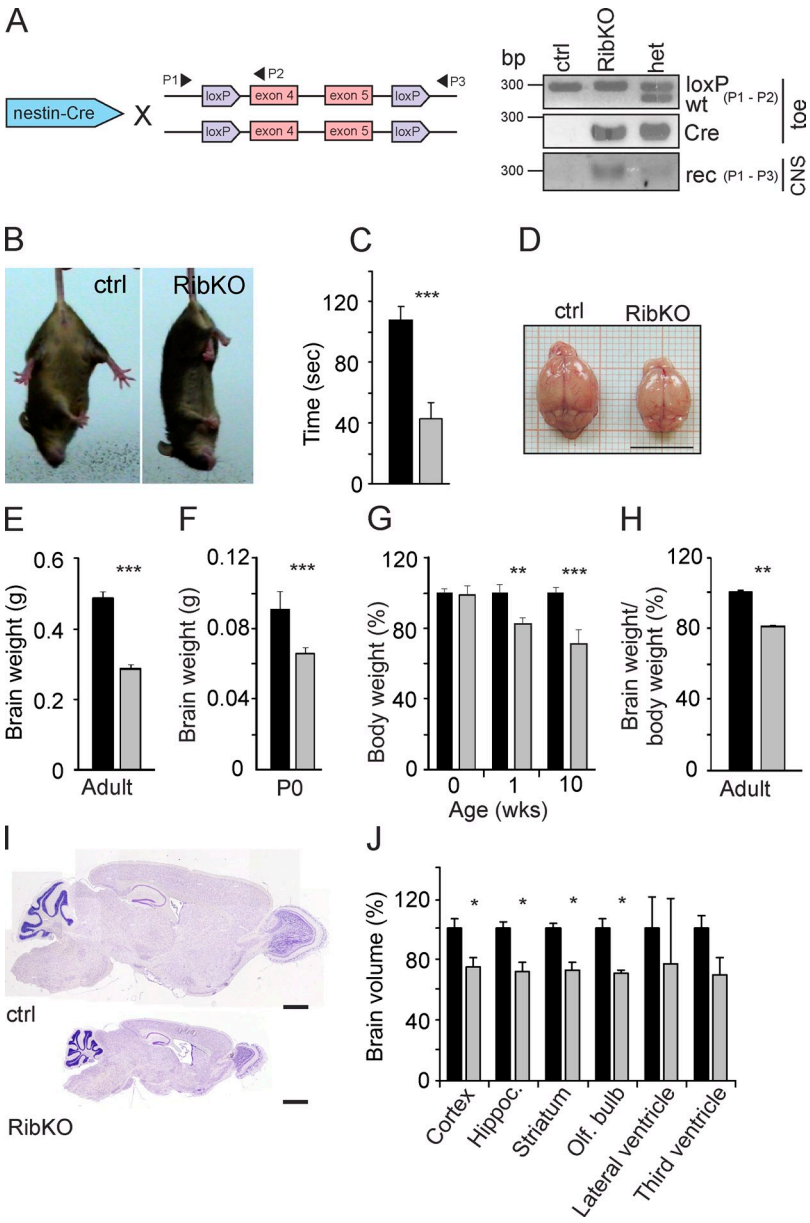

Figure 1. **Rictor knockout in brain causes microcephaly.** (A) Schematic representation of the alleles in the *rictor* gene targeted for nestin-Cre–mediated recombination. PCR primers P1 to P3 are indicated. Right: PCR using genomic DNA from toe lysate of control (ctrl), RibKO, and heterozygous (het) mice to detect the wild-type (wt), the floxed allele (loxP), and Cre. PCR using brain tissue (CNS) and primers P1 and P3 shows successful recombination. (B) Representative images of a control and a RibKO mouse during tail suspension in the clasping test. (C) Average time until control (black bar) or RibKO mice (gray) fell off the rotarod that accelerated from 5 to 30 rpm during 2 min. (D) Photograph of brains from adult control and RibKO mice. (E and F) Quantification of the relative brain weight of adult and newborn (P0) mice. Data represent mean ± SEM with $n = 7$ (adult, control); $n = 6$ (adult, RibKO); $n = 26$ (P0, control); and $n = 7$ (P0, RibKO). (G) Body weight of control and RibKO mice at different postnatal ages. Data represent mean ± SEM with $n = 13$ (P0, control); $n = 8$ (P0, RibKO); $n = 8$ (P7, control); $n = 5$ (P7, RibKO); $n = 10$ (10 wk, control); and $n = 13$ (10 wk, RibKO). (H) Brain weight relative to body weight in the adult. Data represent mean ± SEM with $n = 7$ (control) and $n = 6$ (RibKO). (I) Cresyl violet staining of mid-sagittal sections of brains from adult RibKO and control mice. (J) Quantification of the volumes of several brain regions from 1-yr-old mice. Data represent mean ± SEM with $n = 3$ mice for each genotype. Black bars denote controls, light gray bars denote RibKO mice. Statistical analysis used Student's *t* test: ***, $P < 0.001$; **, $P < 0.01$; *, $P < 0.05$. n.s., nonsignificant; $P \geq 0.05$. Bars: (D) 1 cm; (I) 1 mm.

~40% less than those from littermate controls (Fig. 1 E). Although less striking than in the adult, the brains of newborn RibKO mice were already significantly lighter (Fig. 1 F). In contrast to brain, the total body weight of newborn RibKO mice was still the same as in controls, but RibKO mice did not gain weight like controls so that they became significantly lighter after one week and remained lighter throughout adulthood (Fig. 1 G). Nevertheless, the brains of the RibKO remained significantly and disproportionally lighter (Fig. 1 H). Mid-saggital sections of cresyl violet–stained brains showed that the effect on brain size was rather uniform and affected all brain regions (Fig. 1 I). This uniformity in the size difference was further confirmed by measuring the relative volume of different brain regions using cresyl violet–stained coronal paraffin sections (Fig. 1 J). In contrast to the brain proper, the ventricles were not smaller in RibKO mice (Fig. 1 J). These data thus show that deletion of *rictor* results in a smaller brain, which already manifests at birth. Moreover, the weight difference between RibKO and control brains is larger than the difference in body weight in the adult. These results suggest a direct role of mTORC2 in the control of brain size. RibKO mice also show a strong motor phenotype, indicating that neuronal connectivity in some brain regions might be impaired.

Cells are smaller in rictor-deficient brains

To determine the reasons for the difference in brain size of RibKO mice, we first investigated the proliferation capacity of stem/progenitor cells. To this end, primary neurospheres isolated from newborn pups were cultured for 4 d, followed by trypsinization and resuspension into single cells. The secondary neurospheres were then cultured for another 6 d. The size of the secondary neurospheres from RibKO mice was the same as those isolated from controls (Fig. 2 A) and the number of BrdU-positive cells, when labeled for 24 h before analysis, was indistinguishable (Fig. 2 B). These results indicate that proliferation of stem/progenitor cells

Published April 8, 2013

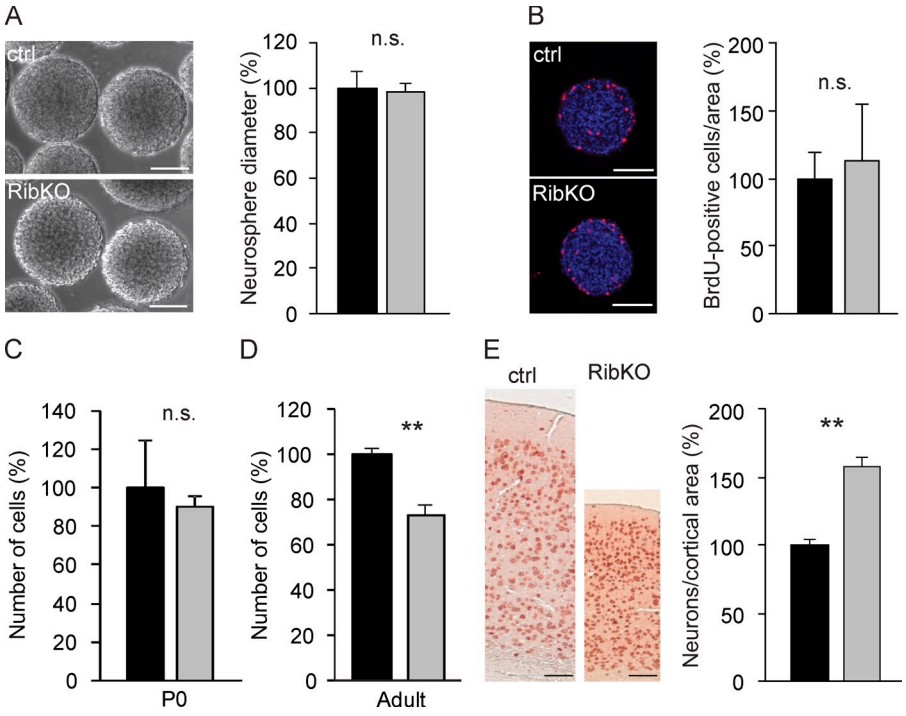

Figure 2. **Changes in cell density in rictor-deficient brains.** (A) Brightfield images of secondary neurospheres isolated from P0 mice, split into single cells after 4–5 d in culture and grown for another 6 d (left), and quantification of the neurosphere diameter (right). Data represent mean ± SEM from n = 613 spheres (control) and n = 583 spheres (RibKO); n = 5 mice for each genotype. (B) Cross sections at the mid-region of neurospheres, stained with antibodies to BrdU (red) and with Hoechst (blue). Neurospheres were labeled with BrdU for 24 h. Quantification of the number of BrdU-labeled cells (right). Data represent mean ± SEM from n = 3 mice per genotype. (C and D) Quantification of the total number of cells in the brains of P0 and adult mice using isotropic fractionation. Data represent mean ± SEM from n = 3 mice per genotype. (E) Picture of cortex sections of adult control and RibKO mice stained with antibodies to NeuN (left) and quantification of neuron density (right). Data represent mean ± SEM from n = 36 areas (control) and n = 3 mice (control), and n = 58 areas and n = 4 RibKO mice. Black bars denote controls, light gray bars denote RibKO mice. Statistical analysis used Student's t test: **, $P < 0.01$. n.s., nonsignificant; $P \geq 0.05$. Bars (A, B, and E) 100 µm.

in RibKO mice is not affected. Likewise, despite the reduced brain weight, the number of cells in brains isolated from newborn RibKO mice was not significantly different from controls (Fig. 2 C). In contrast, the number of cells was lower in adult RibKO mice (Fig. 2 D). The difference in cell number at the adult stage seemed not to be due to increased apoptosis, as the number of cleaved caspase3-positive cells did not differ between the cortex of RibKO and control mice (Fig. S1 A). The number of caspase3-positive cells was, however, rather low and the data varied substantially between animals, which does not allow to exclude the possibility that RibKO mice might be more affected by apoptosis.

To assess whether cell size might cause the difference in brain size, we next stained sagittal sections with antibodies directed against the neuron-specific antigen NeuN. These antibodies strongly stain the nuclei and more weakly the cytoplasm of neurons. As shown in Fig. 2 E, the density of neurons in the retrosplenial and visual cortex of 9-wk-old RibKO mice was more than 1.5 times higher than in controls. This difference in neuron density was already clearly detected in postnatal day (P7) RibKO mice (Fig. S1 B). These data therefore show that loss of rictor in the brain affects neuron density but not proliferation of cells.

To get a more detailed view on the effect on neuron size in RibKO mice, we next reconstructed the shape of single hippocampal neurons using Golgi staining. Examination of pyramidal neurons in the CA1 region (Fig. 3 A) and quantification of their size by the tracing of single neurons using a Neurolucida camera revealed that the mean total dendritic length of both the apical and basal dendrites was reduced by ~15% (Fig. 3 B). This effect could be reproduced in cultured hippocampal neurons that were isolated from P0 brains, transfected with GFP-expression constructs at day in vitro (DIV) 7 (to visualize individual neurons), and examined at DIV 14 (Fig. 3 C). Quantification revealed

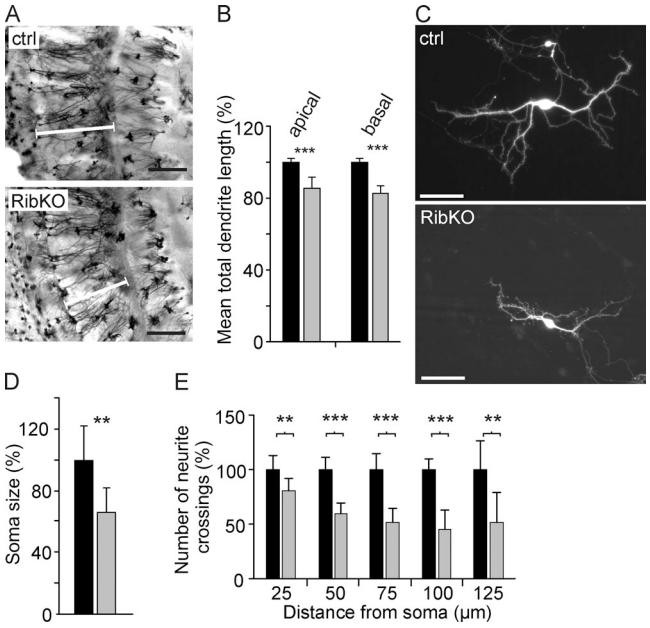

Figure 3. **Rictor regulates neuron size.** (A) Cross sections of hippocampus after Golgi impregnation. The white bar indicates the length of CA1 pyramidal dendrites. (B) Quantification of the mean length of Neurolucida-reconstructed apical and basal dendrites. Data represent mean ± SEM from n = 38 control neurons, n = 32 RibKO neurons derived from 4 different mice of each genotype. (C) Dissociated hippocampal neurons derived from P0 mice, transfected with GFP after 7 d, and grown for 14 d. (D) Mean soma size of hippocampal neurons from dissociated cultures at DIV 14. Data represent mean ± SD from n = 6 mice per genotype. (E) Sholl analysis of hippocampal neurons at DIV 14. Data represent mean ± SD from n = 6 mice per genotype. Black bars denote control, light gray bars denote RibKO mice. Statistical analysis used Student's t test: ***, $P < 0.001$; **, $P < 0.01$. Bars: (A) 200 µm; (C) 50 µm.

Published April 8, 2013

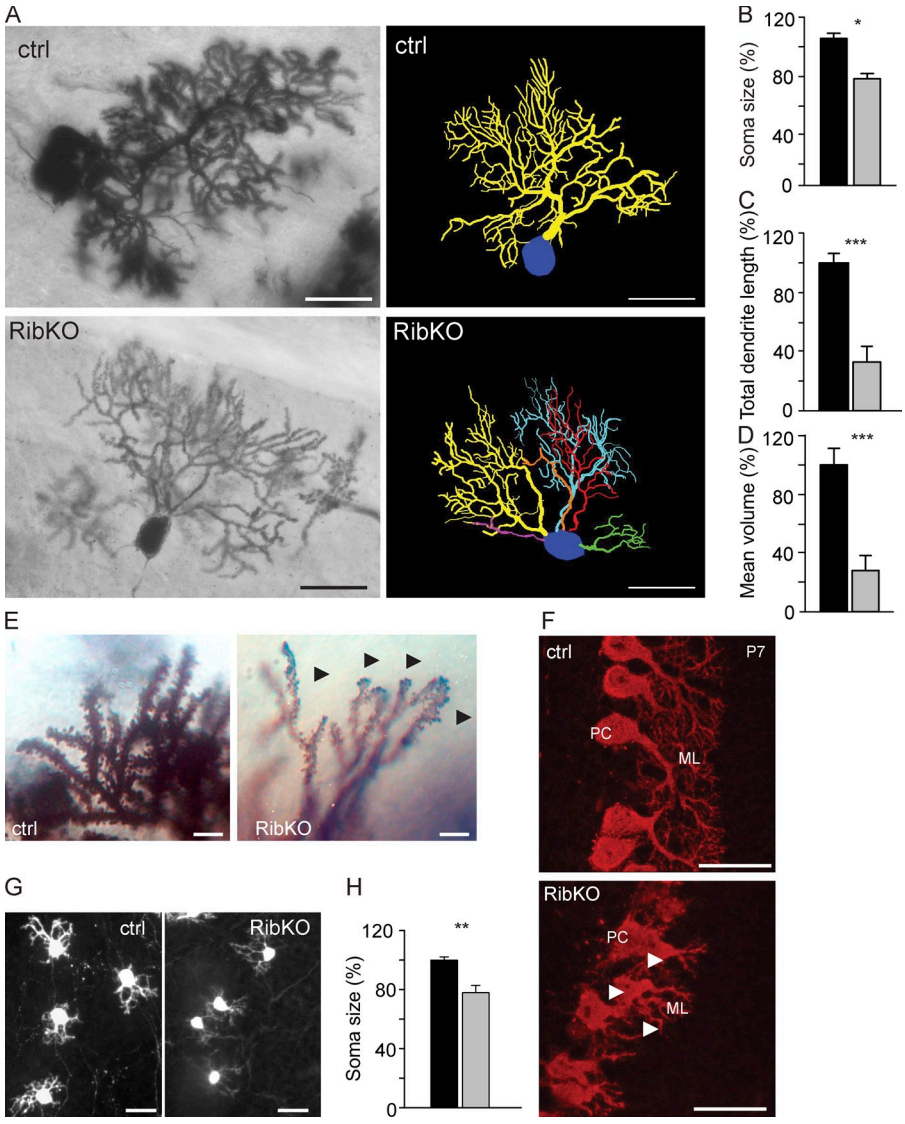

Figure 4. **Rictor is involved in the regulation of Purkinje cell size and shape.** (A) Golgi-stained Purkinje cells from adult control and RibKO mice (left) and reconstruction of a Purkinje cell using Neurolucida. Primary dendrites are indicated by different colors. Examples of a dendritic tree with little or no higher order branches are depicted in purple and orange. (B) Quantification of Purkinje cell soma size. The cell soma perimeter was measured in sections stained with antibodies to calbindin. Data represent mean ± SEM from $n = 4$ mice per genotype. (C) Quantification of the mean Purkinje cell dendrite length and (D) the mean dendrite volume in Neurolucida-reconstructed cells. Data represent mean ± SEM from $n = 4$ mice per genotype. (E) High magnification picture of Purkinje cell terminals of Golgi-stained preparations. Purkinje cell dendrites are often deformed (black arrows) and appear to have fewer spine-like structures. (F) Neurons of P7 stained with antibodies to calbindin. White arrows mark misshaped dendritic trees in RibKO mice. (G) Purkinje cells in organotypic cerebellar slice cultures derived from P0 mice and cultured for 14 d, stained with antibodies to calbindin. (H) Quantification of the soma size of Purkinje cells in organotypic cultures. Data represent mean ± SEM from $n = 4$ (control) and $n = 3$ RibKO mice. Black bars denote control, light gray bars denote RibKO mice. Statistical analysis used Student's *t* test: ***, $P < 0.001$; **, $P < 0.01$; *, $P < 0.05$. PC, Purkinje cell; ML, molecular layer. Bars: (A and G) 50 µm; (F) 20 µm; (E) 10 µm.

that the soma size of RibKO neurons was only ~ 70% of control neurons (Fig. 3 D) and Sholl analysis at DIV 14 showed a highly significant decrease in the complexity of the neurites (Fig. 3 E). These experiments thus indicate that changes in neuron size in RibKO mice are rather a consequence of cell-intrinsic changes than of alterations in the surroundings (e.g., changes in glial cells).

Cerebellar phenotype of RibKO mice

Rictor expression is highest in Purkinje cells of the cerebellum (Shiota et al., 2006) and RibKO mice show an ataxia-like phenotype (Fig. 1, B and C). To see whether loss of rictor would affect Purkinje cells, we next analyzed single cells from Golgi-stained preparations (Fig. 4 A). Reconstruction of cells by tracing them using a Neurolucida camera revealed several distinct structural alterations. One of the most striking differences between Purkinje cells from RibKO and control mice was an increase in the number of primary dendrites. Whereas control neurons always had one primary dendrite, Purkinje cells from RibKO mice often contained two to six primary dendrites (see Neurolucida drawing in Fig. 4 A). Quantification of the size of the Purkinje cells showed a significant decrease in soma size (Fig. 4 B) and a decrease in the length and the volume covered by single dendrites (Fig. 4, C and D). Examination of the Purkinje cell dendrites at high magnification revealed that the thickness of the dendrites was often irregular, fluctuating from very thin to rather thick (swollen) regions (Fig. 4 E, arrows). Thus, deletion of *rictor* causes multiple changes in Purkinje cells that affect the size of the somata and of the dendrites and increases the number of primary dendrites.

To examine whether any of the structural changes could already be observed at early stages of development, we examined the cerebella at P7. In the first postnatal week, Purkinje cells migrate into the periphery and start to align in a monolayer. At that stage, most cells have formed one primary dendrite, which spreads out perpendicularly to the pial surface into the molecular layer where it forms numerous side branches (Kapfhammer, 2004). This alignment and spreading of the primary dendrites was well visible in control mice (Fig. 4 F), whereas the dendrites of Purkinje cells in RibKO mice appeared swollen (arrows) and several

Published April 8, 2013

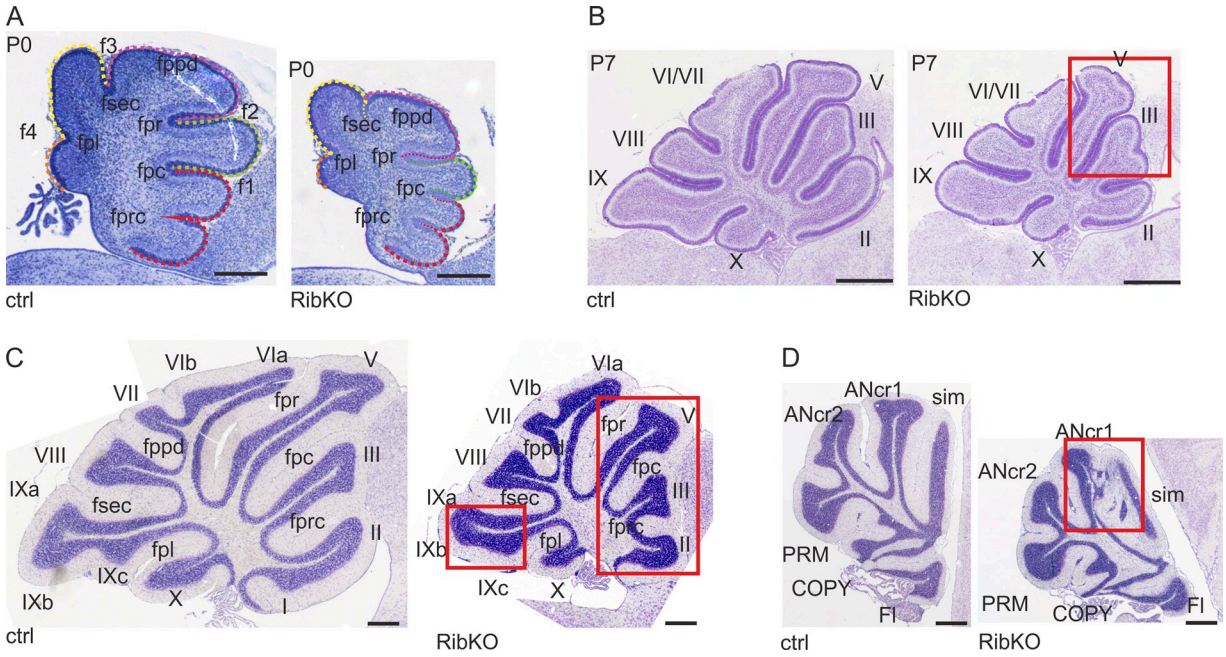

Figure 5. **Rictor deficiency leads to foliation defects in the cerebellum.** (A) Cresyl violet staining of cerebella from P0 control and RibKO mice. (B) Cresyl violet–stained, mid-sagittal sections of P7 cerebella from control and RibKO mice. (C) Sagittal sections of cerebellar vermis from adult control and RibKO mice stained with cresyl violet. (D) Sagittal sections of the lateral cerebellar lobules of adult control and RibKO mice. Foliation defects are marked by red inserts. Fpl, posterolateral fissure; fsec, secondary fissure; fppd, prepyramidal fissure; fpr, primary fissure; fprc, precentral fissure. Vermal lobules are numbered from I to X. Lateral lobules: Ancr, Ansiform cruciform lobule; COPY, Copula pyramidis; Fl, Flocculus; PRM, paramedian lobule; Sim, simple lobule. Bars: (A and B) 250 µm; (C and D) 1 mm.

primary dendrites emerged from the cell bodies (Fig. 4 F). The aberrant Purkinje cell morphology was also reproduced in slice cultures derived from newborn mice and cultured for 14 d. There, the somata of RibKO Purkinje cells were significantly smaller (Fig. 4, G and H). As Purkinje cells in culture retain several primary dendrites because of the lack of climbing fiber innervation (Kapfhammer, 2004), the difference in the number of primary dendrites between RibKO and control mice could not be seen. In summary, these results show that RibKO mice display pronounced structural changes in their Purkinje cells, the most prominent ones being changes in dendritogenesis and overall cell size.

The changes in Purkinje cell size and shape in RibKO mice observed at early postnatal stages suggested to us that mTORC2 might also be involved in cerebellar development and maturation. It is known that mice with defects in Purkinje cells may develop simplified lobule patterns (Sidman et al., 1962; Wetts and Herrup, 1982). Moreover, the structure of the cerebellar lobes is highly conserved and aberrations in their morphology often correlate with defects in motor behavior (Sillitoe and Joyner, 2007). To test whether this would also be the case in RibKO mice, we analyzed the overall structure of the cerebellum. At birth (P0), the cerebellum only consists of the 5 cardinal lobes, which will then develop into 10 mature lobules within the following 21 d (Larsell, 1952). In cerebella of newborn RibKO mice, lobule formation was unchanged (Fig. 5 A). At P7, cerebellar defects became clearly visible as the cerebella were smaller and the structure of lobules III to VII of the cerebellar vermis in RibKO mice already deviated from that of control mice (Fig. 5 B). In 8–10-wk-old RibKO mice, the size of the cerebellum was strongly decreased (Fig. 5 C) and most lobules appeared shortened and the cells seemed more densely packed than in control mice. Moreover, in some regions, changes in the structure of the lobules could be detected. The cerebellar hemisphere was even more affected than the cerebellar vermis. There, both the simple lobule (Sim) and the Ansiform cruciform lobule 1 (ANcr1) were not properly formed and appeared to be fused so that they could not be distinguished as separate lobules (Fig. 5 D). Thus, deletion of *rictor* caused structural changes in the cerebellar morphology. As RibKO mice also show changes in motor behavior, the morphological alterations of the cerebellum might underlie these defects.

Synaptic defects in RibKO mice

The structural changes in the Purkinje cells of RibKO mice suggested that synaptic connectivity might also be affected. To test this, we visualized the Purkinje cells with antibodies to calbindin and the presynaptic terminals of the climbing fibers, which synapse onto Purkinje cells, with antibodies to the vesicular glutamate transporter protein 2 (vGLUT2; Fremeau et al., 2001; Hisano et al., 2002). The density of vGLUT2-positive puncta in the molecular layer was decreased in RibKO mice (Fig. 6 A). The number of synaptic inputs from parallel fibers onto Purkinje cells was estimated by Western blot analysis using antibodies against the vesicular glutamate transporter vGLUT1, which is enriched in parallel fiber synapses (Fremeau et al., 2001; Hisano et al., 2002). Compared with control lysates, vGLUT1-like immunoreactivity was reduced to less than 80% in RibKO mice (Fig. 6 B). These results therefore indicate that both excitatory inputs onto Purkinje cells are altered in RibKO mice.

To test for functional differences, we next measured miniature excitatory postsynaptic currents (mEPSCs) and miniature

Published April 8, 2013

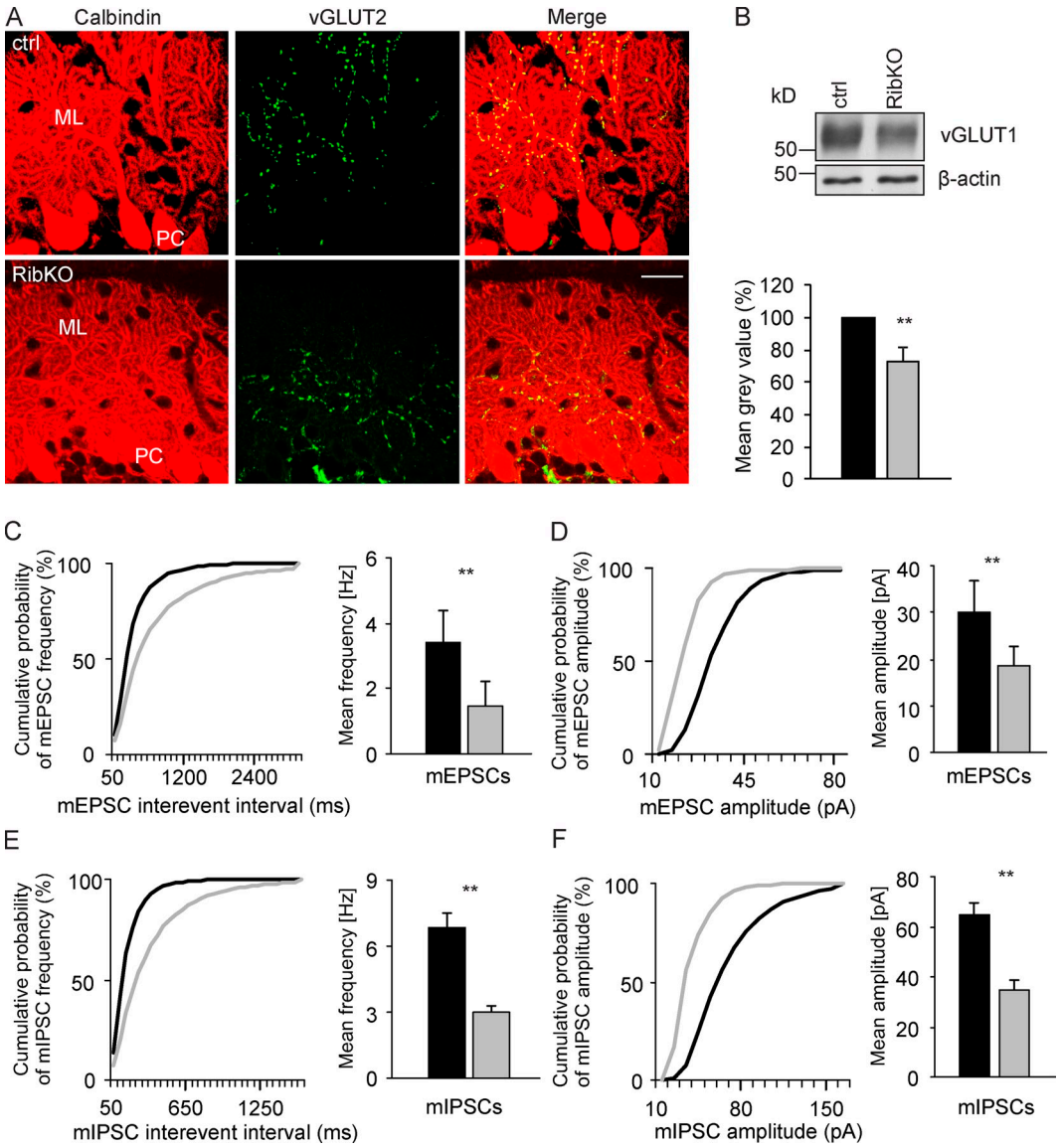

Figure 6. **Synaptic functions are altered in Purkinje cells of RibKO mice.** (A) Confocal image of cerebellar vermal lobule III of adult control and RibKO mice stained with antibodies to calbindin to visualize Purkinje cells (PC, red) and antibodies to vGLUT2 for climbing fiber terminals (green). ML, molecular layer. (B) Western blot analysis of vGLUT1 in cerebellar lysates of control and RibKO mice and corresponding quantification of the mean gray values. β-Actin was used as loading control. Data represent mean ± SEM from $n = 6$ control and $n = 7$ RibKO mice. (C and D) Miniature excitatory postsynaptic currents (mEPSCs) and (E and F) miniature inhibitory postsynaptic currents (mIPSCs) recorded from Purkinje cells in acute sagittal slices of 25-d-old control and RibKO mice. Data represent mean ± SEM from $n = 4$ control and $n = 3$ RibKO mice. Black bars/lines are from control; gray bars/lines are from RibKO mice. Statistical analysis used Student's *t* test: **, $P < 0.01$. Bar, 20 µm.

inhibitory postsynaptic currents (mIPSCs) in single Purkinje cells using the patch-clamp technique. As expected from the histological assessment, the inter-event interval of the mEPSCs was strongly increased in Purkinje cells from RibKO mice, which resulted in the lowering of the mEPSC frequency by about half (Fig. 6 C). In addition, the amplitude of the mEPSCs was reduced in RibKO mice as seen by the leftward shift in the cumulative probability curve and the decrease of the mean mEPSC amplitude (Fig. 6 D). Recordings of the inhibitory synaptic input revealed that both the frequency and the amplitude of mIPSCs were reduced in RibKO mice to an extent that was quite similar to that observed for the mEPSCs (Fig. 6, E and F). In summary, these results show that synaptic connectivity of Purkinje cells in the cerebellum of RibKO mice is strongly affected, suggesting that these synaptic changes might be the basis for the ataxia-like phenotype of RibKO mice.

Biochemical analysis of RibKO mice

Our findings that deletion of *rictor* results in a microcephalic phenotype and a decrease in the size of neurons is rather unexpected, as such an effect has not been documented in other tissue upon *rictor* deletion. In stark contrast, deletion of mTORC1 has strong effects on organ and cell size (Russell et al., 2011). To investigate whether mTORC1 signaling was also affected in the RibKO mice and to unravel the molecular mechanisms that underlie the different aspects of the phenotype in RibKO mice,

Published April 8, 2013

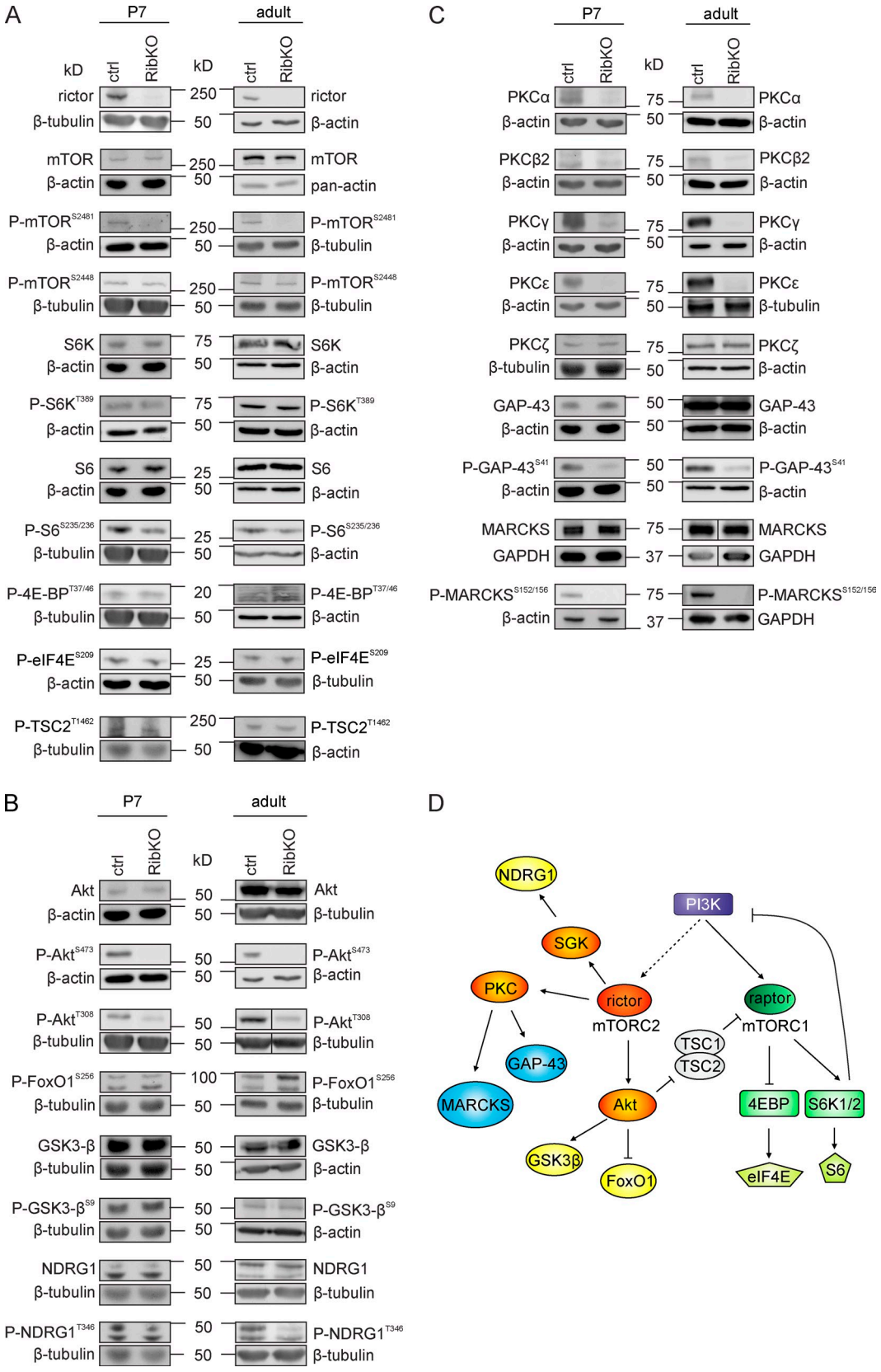

Figure 7. **Biochemical analysis of RibKO mice indicates altered activation of AGC kinases but not of mTORC1.** (A–C) Western blot analysis of brain lysates from P7 and adult control and RibKO mice. β-Tubulin, GAPDH, β-actin, or pan-actin were used as loading controls. Some loading controls are intentionally shown more than once because experimental data were derived from the same SDS gel. (A) Detection of the phosphorylation levels of proteins involved in mTORC1 and mTORC2 signaling. Please note that phosphorylation levels of mTOR at Ser2481 and Ser2448 in adult mice showed a substantial variation. The P-mTOR(S2481) and P-mTOR(S2448) bands shown are representative for the averaged band intensities of all tested mice (see Table 1). (B) Phosphorylation

Published April 8, 2013

we analyzed brain lysates of P7 and adult mice using Western blot analysis. As expected from nestin-Cre–mediated recombination that affects all precursor cells of the CNS (Tronche et al., 1999; Graus-Porta et al., 2001), rictor protein could not be detected in brain lysates from adult RibKO mice and was significantly reduced in P7 RibKO brain lysates (Fig. 7 A; see Table 1 for quantification). The loss of rictor did not affect the levels of mTOR but abrogated phosphorylation of mTOR at the mTORC2-specific residue Ser2481 (Fig. 7 A; Table 1). Importantly, all the phosphorylation sites indicative of mTORC1 signaling were not altered in RibKO mice. These included phosphorylation of mTOR at Ser2448, of S6K and its substrate S6, and of 4E-BP and its substrate elongation initiation factor 4E (eIF4E). In addition, phosphorylation of tuberous sclerosis complex 2 (TSC2), a downstream target of Akt and upstream inhibitor of mTORC1, was also not altered (Fig. 7 A; Table 1). These results indicate that inactivation of mTORC2 in the developing and adult brain does not affect mTORC1 activity and thus suggests that an mTORC1-independent mechanism is responsible for the microcephaly in RibKO mice.

Previous work has shown that mTORC2 affects phosphorylation of AGC kinases including Akt (Sarbassov et al., 2005), SGK1 (García-Martínez and Alessi, 2008), and PKC (Facchinetti et al., 2008; Ikenoue et al., 2008). Although the protein levels of Akt were not changed in comparison to control mice, phosphorylation at Ser473 was strongly diminished in RibKO mice (Fig. 7 B; Table 1). Phosphorylation of Akt at Thr308 was reduced in RibKO mice but reached significance only in the adult brain. However, activation of the Akt downstream targets FoxO1 and GSK3-β was unchanged (Fig. 7 B; Table 1). These results indicate that Akt activation toward the mTORC1, the GSK3-β, and the FoxO1 branch was not altered in RibKO mice despite the lower levels of phosphorylation at Ser473. Activation of SGK1, as indicated by the phosphorylation of its downstream substrate, N-myc downstream regulated gene 1 (NDRG1), was decreased in the adult but not in the brains of P7 RibKO mice (Fig. 7 B; Table 1).

As mTORC2 was also shown to regulate phosphorylation and thereby protein levels of certain isoforms of PKC (Facchinetti et al., 2008; Ikenoue et al., 2008), we also tested brain lysates of RibKO mice for changes in PKC. There are at least nine different isoforms that are grouped into three classes based on their structural and enzymatic properties. These include the conventional isoforms (PKCα, -β, and -γ), the novel isoforms (PKCε, -δ, and -η), and the atypical isoforms (PKCζ, -λ, -ι, and -μ). The conventional PKC isoforms are activated by phosphorylation and second messengers (elevated Ca^{2+} concentrations and diacylglycerol [DAG]), whereas the novel isoforms are regulated only by DAG and phosphorylation (Ohno and Nishizuka, 2002). In P7 and adult RibKO mice, phosphorylation and protein levels of all three conventional PKCs and the novel PKCε was strongly decreased (Fig. 7 C; Fig. S2; Table 1). In contrast, the atypical isoform PKCζ was not affected (Fig. 7 C; Table 1). The strong decrease in PKCs had functional consequences, as phosphorylation levels of the well-known downstream substrates GAP-43 and MARCKS were much lower in RibKO mice than in controls (Fig. 7 C; Table 1). In conclusion, this biochemical analysis indicates that the growth defect in RibKO mice is a consequence of changes in downstream substrates of mTORC2 and not by affecting mTORC1 signaling. In addition, loss of rictor leads to the profound loss of several PKC isoforms in the brain, which has not been reported for other tissues.

Purkinje cell–specific deletion of *rictor*

As RibKO mice lack rictor in all cells of the CNS, this animal model cannot answer if the observed phenotypes were the consequence of cell-autonomous function of mTORC2 or a consequence of altered cell–cell communication. To address this question, we crossed floxed *rictor* mice with mice in which the Cre recombinase was knocked-in into the *L7/Pcp-2* locus (Fig. 8 A; Saito et al., 2005). *L7/Pcp-2-Cre* mice start to express the Cre recombinase during late embryogenesis and its expression is restricted to Purkinje cells in a mosaic pattern (Saito et al., 2005). Offspring that was heterozygous for *L7/Pcp-2-Cre* and homozygous for the floxed *rictor* allele (called RiPuKO$^{Cre/+}$ for *rictor* Purkinje cell knockout) were born in a Mendelian ratio and mice could not be distinguished from their control littermates. Successful recombination of the floxed alleles in Purkinje cells was indicated by the significant loss of rictor and of PKCγ from cerebellar lysates of adult RiPuKO$^{Cre/+}$ mice (Fig. 8 B). Staining of sagittal cerebellar sections of adult RiPuKO$^{Cre/+}$ mice with antibodies to calbindin and PKCγ revealed that ∼1/3 of the cells were negative for PKCγ (Fig. 8 C; Fig. S3 A). The proportion of PKCγ-negative Purkinje cells increased to ∼3/4 when mice were made homozygous for the *L7/Pcp-2-Cre* allele (Fig. S3 A). In contrast, Purkinje cells from mice lacking *L7/Pcp-2-Cre* were all PKCγ positive (Fig. 8 C; Fig. S3 A). These results indicate that Cre expression in Purkinje cells is indeed mosaic and that an increase in gene dosage for the Cre recombinase results in a higher rate of excision of the floxed alleles.

To assure that PKCγ-negative Purkinje cells were indeed deficient for rictor, single Purkinje cells were labeled with biocytin during whole-cell patch clamping and the mRNA was analyzed by single-cell RT-PCR (Sucher et al., 2000). The biocytin-labeled Purkinje cells were then stained with antibodies to PKCγ and staining results were compared with those from single-cell RT-PCR. As shown in Fig. S3 B, out of the nine cells analyzed all the PKCγ-negative cells also expressed *rictor* transcripts lacking exons 4 and 5 (Fig. S3 B). There was one cell that was still positive for PKCγ even though only mRNA for the recombined *rictor* locus was amplified (Fig. S3 B; cell #7). These experiments show that all the PKCγ-negative Purkinje cells are deficient for rictor, whereas the majority of the PKCγ-positive cells are rictor positive.

Morphological analysis of Purkinje cells from RiPuKO$^{Cre/+}$ and RiPuKO$^{Cre/Cre}$ mice showed that the somata of the PKCγ-negative

of mTORC2 targets Akt and SGK1 and downstream targets. (C) Western blot analysis of several PKC isoforms and the PKC targets GAP-43 and MARCKS. Levels of MARCKS showed considerable variations in adult mice. The shown bands are representative for the averaged band intensities of all tested mice (see Table 1). (D) Schematic view of the signaling mechanisms up- and downstream of mTORC1 and mTORC2.

Published April 8, 2013

Table 1. **Quantification of Western blot analyses**

Antibody target	P7 brain		Adult brain	
	Control	RibKO	Control	RibKO
rictor	100 ± 8.1	13.7 ± 2.4***	100 ± 24	n.d.
mTOR	100 ± 10.5	108.5 ± 7.9	100 ± 31	64.9 ± 7.5
P-mTOR (Ser2481)	100 ± 2.8	21.2 ± 5***	100 ± 25.2	2.7 ± 2.2**
P-mTOR (Ser2448)	100 ± 7	96.5 ± 12.3	100 ± 20.7	79 ± 21
S6K	100 ± 12.2	93.6 ± 8.2	100 ± 8.8	91.4 ± 5.8
PS6K (Thr389)	100 ± 8.3	116.5 ± 5.9	100 ± 5.2	85.6± 9.2
S6	100 ± 9.1	107.2 ± 13.8	100 ± 6.1	169.3 ± 29.4
P-S6 (Ser235/236)	100 ± 6.2	83.2 ± 3.3	100 ± 10	105.2 ± 17.5
P-4E-BP (Thr37/46)	100 ± 8.3	94 ± 7.6	100 ± 11	179.7 ± 37.2
P-eIF4E (Ser209)	100 ± 13	84.6 ± 3.1	100 ± 10	107.0 ± 13.8
P-TSC2 (Thr1462)	100 ± 9.8	177.5 ± 45.6	100 ± 22	80.2 ± 22.4
Akt	100 ± 10.5	127.6 ± 17.3	100 ± 4.7	99.4 ± 6.1
P-Akt (Ser473)	100 ± 10	3.9 ± 0.9***	100 ± 12	18.3 ± 4.8***
P-Akt (Thr308)	100 ± 7	52 ± 17	100 ± 15	36.9 ± 8.1**
P-FoxO1 (Ser256)	100 ± 15.7	141.1 ± 13.3	100 ± 9.3	164.6 ± 26.7
GSK3-β	100 ± 5.0	101.5 ± 5.5	100 ± 5.1	97.1 ± 4.7
P-GSK3-β (Ser9)	100 ± 11.7	115.8 ± 12.4	100 ± 17	103.7 ± 5.1
NDRG1	100 ± 19.8	115.3 ± 6.5	100 ± 5.4	94.2 ± 7.9
P-NDRG1 (T346)	100 ± 13.7	92 ± 15.9	100 ± 3.8	52.4 ± 7.3***
PKCα	100 ± 6.8	55.8 ± 3.4***	100 ± 23.8	2.6 ± 1.7***
PKCβ2	100 ± 7.0	78.6 ± 3.7*	100 ± 11.4	3.7 ± 0.4***
PKCγ	100 ± 6.2	58.5 ± 2.1***	100 ± 6.6	7.4 ± 1.8***
PKCε	100 ± 12	17.7 ± 2.8***	100 ± 22.9	15.5 ± 5*
PKCζ	100 ± 17.1	106 ± 11.9	100 ± 14.6	60.0 ± 7.8
GAP-43	100 ± 1.2	105 ± 5.8	100 ± 5	99.9 ± 6.6
P-GAP-43 (Ser41)	100 ± 13.1	22.4 ± 3.9**	100 ± 27	19.5 ± 4.7**
MARCKS	100 ± 2.3	94.2 ± 3.4	100 ± 22	109.7 ± 3
P-MARCKS	100 ± 8.8	n.d.	100 ± 25	n.d.

Quantification of protein and phosphorylation levels of proteins shown in Fig. 7. Percentage given represents the relative intensity of the protein bands as detected by Western blot analysis from control and RibKO mice. Equal amount of protein was loaded and immunodetection of β-tubulin, GAPDH, β-actin, or pan-actin served as loading control. Amount of each protein listed was normalized to loading control. All values obtained in controls were set to 100%. Data represent mean ± SEM from $n \geq 3$–15 mice for each genotype. n.d., not detected. Student's *t* test: ***, $P < 0.001$; **, $P < 0.01$; *, $P < 0.05$.

cells were significantly smaller than those of Purkinje cells in control mice (Fig. 8, D and E). Importantly, PKCγ-positive Purkinje cells were also significantly bigger than the PKCγ-negative cells in the RiPuKO$^{Cre/+}$ mice (Fig. 8 E). In addition, the average diameter of the primary dendrites of PKCγ-negative Purkinje cells in the RiPuKO$^{Cre/+}$ mice was significantly smaller than in cells from control mice (Fig. 8 F), and PKCγ-negative Purkinje cells in RiPuKO$^{Cre/Cre}$ mice formed in more than 30% of the cases two or more primary dendrites (Fig. 8, D and G). Rictor-deficient (i.e., PKCγ-negative) Purkinje cells that were isolated from RiPuKO$^{Cre/Cre}$ mice and were cultured for 14 d in organotypic slices also displayed aberrations in axon structure compared with PKCγ-positive neurons (Fig. 8 H). In particular, the diameter of the axons was significantly diminished in the PKCγ-negative but not the PKCγ-positive Purkinje cells (Fig. 8 I). Thus, selective elimination of rictor in Purkinje cells causes multiple morphological changes that affect cell size and neurite morphology.

To test whether these morphological changes of the PKCγ-negative Purkinje cells from RiPuKO$^{Cre/Cre}$ mice also affected synaptic properties, we measured mEPSCs and mIPSCs in acute cerebellar slices from 6-wk-old mice. The single-cell recordings revealed a strong decrease in the mEPSC frequency (Fig. 9, A and B) and no change in the amplitude (Fig. 9 C). In contrast, the mIPSC frequency in control Purkinje cells was the same as in PKCγ-negative and PKCγ-positive Purkinje cells in RiPuKO$^{Cre/Cre}$ mice. However, PKCγ-negative cells from RiPuKO$^{Cre/Cre}$ mice showed a reduction in the mIPSC amplitude compared with PKCγ-positive cells from RiPuKO$^{Cre/Cre}$ or from control mice (Fig. 9, E and F). The reduction in mEPSC frequency indicates that RiPuKO$^{Cre/Cre}$ mice have fewer functional excitatory synapses, whereas the reduction in mIPSC amplitude points to a reduction in the number or the functionality of inhibitory receptors at the Purkinje cell membrane. Thus, in contrast to RibKO mice where all parameters of the mEPSCs and mIPSCs are diminished, RiPuKO$^{Cre/Cre}$ mice show changes only in mEPSC frequency and in the mIPSC amplitude. These results therefore suggest that presynaptic input onto Purkinje cells might in addition be affected in RibKO mice because of the broad expression of *nestin-Cre*. In conclusion, specific elimination of mTORC2-associated protein rictor in Purkinje cells using *L7/Pcp-2-Cre* results in the reiteration of several phenotypic distortions observed in RibKO mice, including the reduction of cell size, the change in cell morphology, and in synaptic function. Thus, those common phenotypes are based on a cell-autonomous function of mTORC2.

Published April 8, 2013

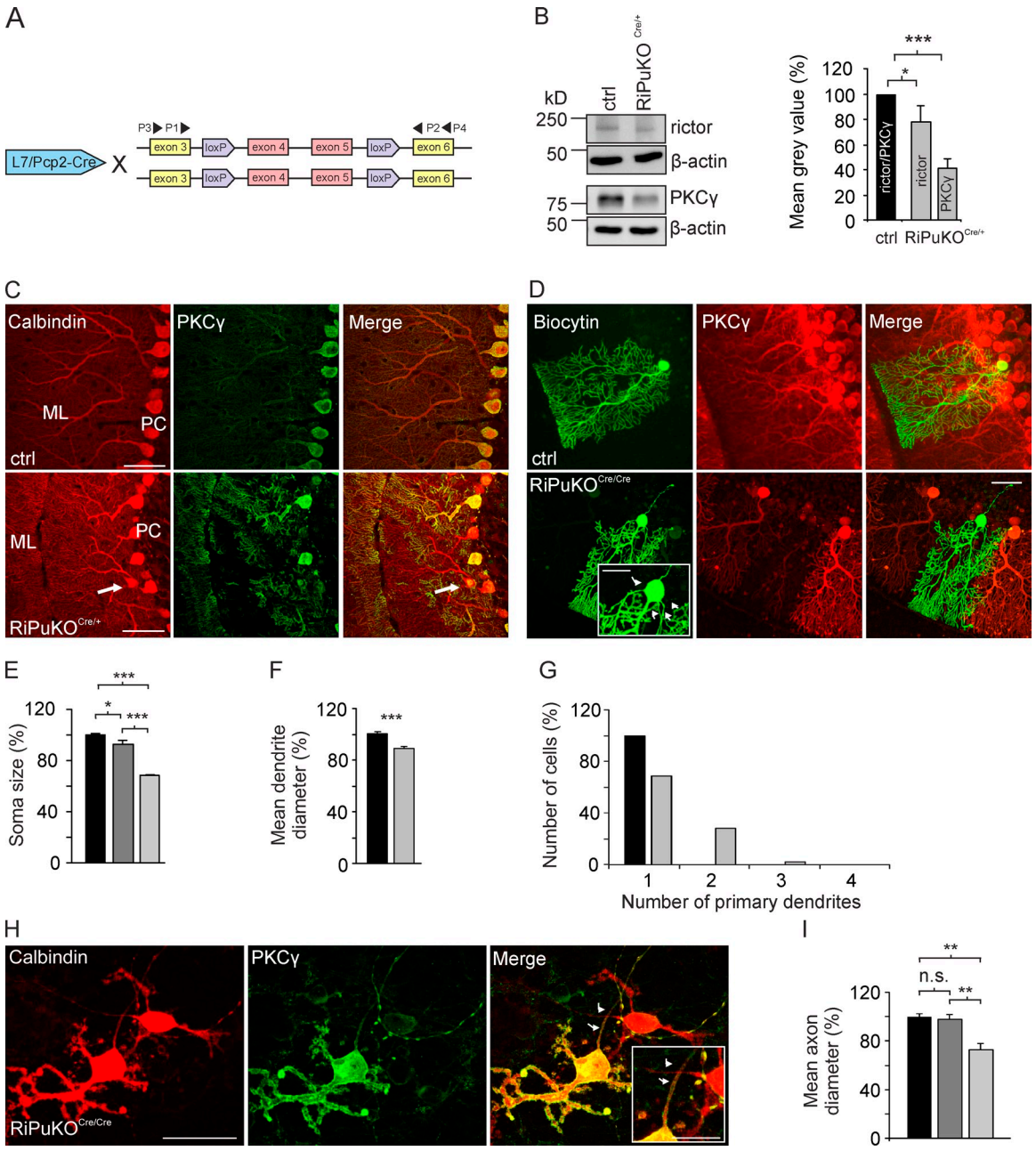

Figure 8. **The role of rictor on cell size and cell morphology is cell-autonomous.** (A) Schematic representation of the genetic organization of mice homozygous for the targeted *rictor* alleles and mice expressing Cre-recombinase from the *L7/Pcp-2* locus. Please note the localization of the primers used to detect *rictor* recombination in single-cell PCR (see Fig. S3). (B) Western blot analysis of cerebellar lysates from adult control and RiPuKO$^{Cre/+}$ mice for rictor and PKCγ (left) and quantification of their mean gray value (normalized to β-actin; right). Values for rictor and PKCγ in controls (ctrl) were set to 100% (black bar). Gray bars represent values for rictor and PKCγ in RiPuKO$^{Cre/+}$ mice. Data represent mean ± SEM from $n = 5$ mice per genotype. (C) Cross section of cerebella stained with antibodies to calbindin (red) and PKCγ (green). PKCγ staining is lost in some, but not all Purkinje cells in RiPuKO$^{Cre/+}$ mice because of the mosaic recombination of the *rictor* allele (see Fig. S3). Some of the PKCγ-negative cells have several primary dendrites, are misaligned, and diverge from the perpendicular plain (white arrow). (D) Immunostaining for PKCγ (red) of biocytin-filled (green) Purkinje cells from control or RiPuKO$^{Cre/Cre}$ mice. Purkinje cells that are negative for PKCγ often have more than one primary dendrite (white arrows). (E) Quantification of the Purkinje cell soma size in control mice (black bar), in PKCγ-positive cells (dark gray), and in PKCγ-negative cells (light gray) from RiPuKO$^{Cre/+}$ mice. Data represent mean ± SEM from $n = 3$ mice for each genotype. (F) Quantification of the Purkinje dendrite diameter in control (black) and PKCγ-negative cells in RiPuKO$^{Cre/+}$ mice (gray). Data represent mean ± SEM from $n = 3$ mice. (G) Quantification of the number of primary dendrites in biocytin-filled Purkinje cells of control (black) and of PKCγ-negative cells from RiPuKO$^{Cre/Cre}$ mice (gray). Numbers derive from $n = 38$ cells of a total of 5 control mice, and from $n = 42$ cells of a total of 7 RiPuKO$^{Cre/Cre}$ mice. (H) Cerebellar slice cultures isolated from RiPuKO$^{Cre/Cre}$ mice and stained for calbindin and PKCγ. The white arrows indicate axons. The inset shows a high magnification picture of those axons. (I) Quantification of the Purkinje axon diameter in cerebellar slice cultures isolated from control mice (black), and PKCγ-positive (dark gray), and PKCγ-negative cells (gray) isolated from RiPuKO$^{Cre/Cre}$ mice. Data represent mean ± SEM from $n = 5$ mice for each genotype. Statistical analysis used Student's *t* test (B and F) or one-way Anova followed by Tukey's test (E and I): ***, $P < 0.001$; **, $P < 0.01$; *, $P < 0.05$. n.s., nonsignificant; $P \geq 0.05$. Bars: (H, inset) 10 µm; (C, H, and inset in D) 25 µm; (D) 50 µm.

Published April 8, 2013

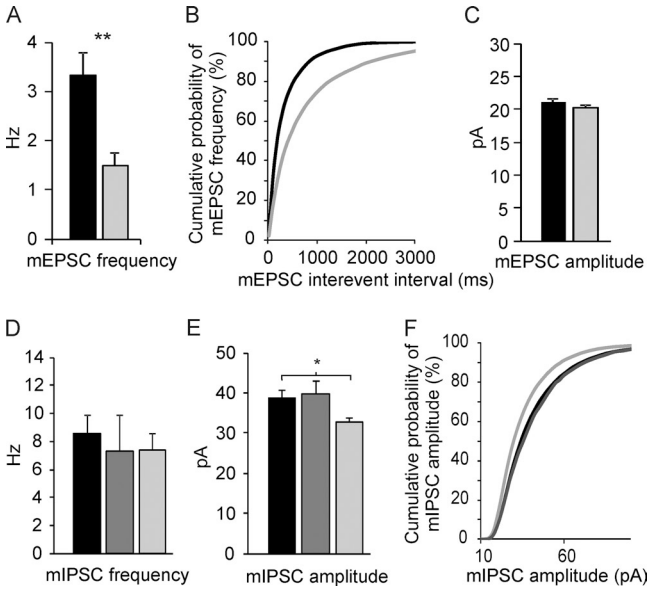

Figure 9. **Altered synaptic properties in Purkinje cells of RiPuKO$^{Cre/Cre}$ mice.** (A and B) Electrophysiological recording of the mean mEPSC frequency in control (black) and PKCγ-negative Purkinje cells of RiPuKO$^{Cre/Cre}$ mice (gray) and (C) the mean mEPSC amplitude in those mice. Data represent mean ± SEM from n = 19 neurons from 5 different control mice and n = 19 cells from 8 different RiPuKO$^{Cre/Cre}$ mice. (D–F) Measurement of the mean frequency (D) and the mean amplitude (E and F) of mIPSCs in Purkinje cells from control mice (black), PKCγ-positive (dark gray), and PKCγ-negative (light gray) cells from RiPuKO$^{Cre/Cre}$ mice. Data represent mean ± SEM from n = 21 cells from 4 different control mice; n = 25 PKCγ-positive cells from 5 RiPuKO$^{Cre/Cre}$ mice; and n = 7 PKCγ-negative cells from a total of 3 RiPuKO$^{Cre/Cre}$ mice. Statistical analysis used Student's t test (A and C) or one-way Anova followed by Tukey's test (D and E): **, $P < 0.01$; *, $P < 0.05$.

Discussion

Germline deletion of *rictor* in mice causes their death around embryonic day 10.5 to 11.5 (Guertin et al., 2006; Shiota et al., 2006). Here we show that deletion of *rictor* in brain precursor cells does not cause early death, indicating that the embryonic lethality in whole-body *rictor* knockout mice is not due to brain abnormalities. We find that RibKO mice have a smaller brain and that this is mainly caused by a reduction in cell size. Moreover, we find a strong phenotype in Purkinje cells that affects the morphology and connectivity of those neurons, both features that might contribute to the motor deficits. Interestingly, a recent publication where exon 3 of *rictor* was deleted using the same nestin-Cre mice linked the phenotype to schizophrenia by demonstrating that the knockout mice were impaired in prepulse inhibition without changes in gross motor function (Siuta et al., 2010). Although this paper reports an interesting aspect of mTORC2 function, the use of the same *nestin* promoter to drive expression of Cre resulted in our hands in a severe phenotype that affected motor behavior and all basic synaptic functions (mEPSCs and mIPSCs) and that did not allow us to test the mice in more elaborated behavioral tasks. We cannot explain the difference between the phenotypes of the two mouse models; one possibility might be that the targeting of exon 3 (Siuta et al., 2010), instead of both exons 4 and 5 (this paper) results in only a partial loss of rictor.

mTORC2 affects cell size

Rictor has been removed in several other organs including skeletal muscle (Bentzinger et al., 2008; Kumar et al., 2008), adipose tissue (Cybulski et al., 2009), and kidney (Gödel et al., 2011). In all those tissues, the phenotype is rather weak and does not affect organ size. Our work now provides strong evidence that deletion of mTORC2 in the entire CNS resulted in a phenotype that was already evident at birth and that affected brain size. This size difference was also seen upon deletion of *rictor* in Purkinje cells, indicating that this function is cell-autonomous. Recent evidence indicates that the morphine-induced decrease in the size of dopaminergic neurons in the ventral tegmental area also involves mTORC2 and that this cell-autonomous effect is rapamycin insensitive (i.e., mTORC1 independent; Mazei-Robison et al., 2011).

Similar size effects in the brain have been reported in mice lacking Akt3/PKBγ, which is the main Akt isoform expressed in the brain (Easton et al., 2005; Tschopp et al., 2005). Although RibKO mice show a strong reduction in the phosphorylation of Akt at Ser473 and some reduction in phosphorylation at Thr308, our biochemical analysis of the mTOR pathway indicates that the growth defect is not based on changes in mTORC1 signaling, as its two downstream targets 4E-BP and S6K and phosphorylation of mTOR at its mTORC1 site Ser2448 were not affected. Although *rictor* deletion does not affect growth in most tissues, such an effect has been described in *Drosophila* (Hietakangas and Cohen, 2007) and in tumors induced by inactivation of the tumor suppressor PTEN (Guertin et al., 2009). Like in our work, signaling to mTORC1 was not affected and under normal conditions, and thus low PI3K signaling, the effect of rictor inactivation on cell growth was rather small or not detectable (Hietakangas and Cohen, 2007; Guertin et al., 2009). The observed microcephaly in the RibKO mice and the reduced cell size in RiPuKO mice might thus be the result of a highly active PI3K pathway in cells of the brain. However, we cannot exclude that the additional downstream targets of mTORC2, such as SGK1 and PKC isoforms, also contribute to the size difference. Such alternative explanations are particularly important as our biochemical analysis did not reveal changes in the activation of the two Akt targets FoxO1 and GSK3-β.

mTORC2 affects neuron morphology

Besides the effect of *rictor* deletion on cell size, we also observed a striking difference in neurite morphology. The most obvious difference to control mice, which was observed in both RibKO and RiPuKO mice, was an increase in the number of primary dendrites in Purkinje cells. Although both SGK1 and Akt have also been implicated in neurite growth (Read and Gorman, 2009), there is no direct evidence for their involvement in the shaping of neurites in Purkinje cells. We therefore hypothesize that those morphological changes are rather due to the loss of PKC isoforms in RibKO and RiPuKO mice. As shown previously, mTORC2 is required for the phosphorylation of some PKC isoforms at the turn motif site (Facchinetti et al., 2008; Ikenoue et al., 2008). This phosphorylation is important for the stability of the protein as nonphosphorylated forms are rapidly degraded by the proteasome pathway (Facchinetti et al., 2008; Ikenoue et al., 2008).

Published April 8, 2013

Our findings that several PKC isoforms are almost undetectable in brain lysates of adult RibKO mice are strong in vivo support for the importance of mTORC2 in stabilizing PKCs. Mutations in PKCγ cause spinocerebellar ataxia (SCA) type 14 (Chen et al., 2003) and as of today, more than 20 causative mutations have been described (Seki et al., 2011). Interestingly, some of the phenotypes described for Purkinje cells expressing those PKC mutants are similar to those observed in RibKO and RiPuKO mice. Most of the PKCγ mutations act in an autosomal-dominant way and it is not clear whether the ataxia is due to a dominant effect or the consequence of a loss of function of those mutants.

We also found that the two PKC substrates GAP-43 and MARCKS were not phosphorylated in RibKO mice. Whereas GAP-43 is well known to affect axon growth and terminal sprouting (Benowitz and Routtenberg, 1997), MARCKS affects dendritic branching (Li et al., 2008) and the morphology and density of postsynaptic spines (Calabrese and Halpain, 2005). Interestingly, the function of MARCKS is modulated by PKC-dependent phosphorylation. Thus, the resemblance of the phenotypes from PKCγ, GAP-43, and MARCKS mutants with those in RibKO or RiPuKO mice indicates that mTORC2 affects neuron morphology via the PKC pathway. The fact that only some aspects of the rictor-deficient phenotype are also observed in PKCγ- or PKCα-deficient Purkinje cells (Metzger, 2010) suggests that a knockout of individual PKC isoforms might be compensated by other isoforms.

Synaptic function

Another interesting result of our work is that synaptic function is also influenced by the deletion of *rictor* from the mouse brain. Because of the very severe morphological changes in the cerebellum of the RibKO mice, it is not that surprising to detect changes in the function of both excitatory and inhibitory synapses. The reduction in the frequency and the amplitude of the mEPSCs also correlated well with the observed changes in synaptic markers. More importantly, we also observed significant changes of synaptic function in the RiPuKO mice and those changes were restricted to Purkinje cells that were negative for PKCγ (i.e., deficient for rictor). While the amplitude of the mEPSCs was not changed in RiPuKO mice, mEPSC frequency was only ∼50% of that in control cells. In contrast, the frequency of the mIPSCs was like in controls but the amplitude was significantly smaller. The finding that a Purkinje cell–specific elimination of rictor differentially affected both excitatory and inhibitory synapses suggests a role of mTORC2 in synaptic homeostasis. Interestingly, homeostatic adaptation of synapses is discussed as a mechanism that contributes to the overall changes upon sustained exposure to morphine, and mTORC2 has been implicated in this process (Mazei-Robison et al., 2011).

In summary, our data show that mTORC2 has an important function in neurons and thus the removal of rictor from brain results in a considerably more severe phenotype than its inactivation in other tissues. Although our results on nestin-Cre–mediated *rictor* deletion suggest that mTORC2 might have similar functions in different neurons, it will be important in the future to analyze other neuron-specific *rictor* knockout models for the contribution of mTORC2 to specific psychiatric and neurological diseases.

Materials and methods

Generation of mice

Mice, homozygous for an allele containing LoxP sites flanking exon 4 and 5 of the *rictor* gene were crossed with nestin-Cre transgenic mice (B6.Cg-Tg(Nes-cre)1Kln/J; The Jackson Laboratory). These mice were then crossed with homozygously floxed *rictor* mice ($rictor^{fl/fl}$) to obtain RibKO mice ($rictor^{fl/fl}$; Tg(Nes-cre). Littermates that either lacked Cre ($rictor^{fl/fl}$) or were heterozygous for the floxed allele ($rictor^{fl/+}$; Tg(Nes-cre)) were used as controls. Purkinje cell–specific knockouts (RiPuKO mice) were obtained by crossing mice where *Cre* was knocked into the *L7/Pcp-2* locus (Saito et al., 2005) with $rictor^{fl/fl}$ mice. Further crossing yielded mice that carried two floxed *rictor* alleles and were heterozygous or homozygous for *L7/Pcp-2*-Cre and are referred to as $RiPuKO^{Cre/+}$ or $RiPuKO^{Cre/Cre}$, respectively. Control mice for $RiPuKO^{Cre/+}$ mice were ($rictor^{fl/fl}$; $L7/Pcp\text{-}2^{+/+}$). Controls for $RiPuKO^{Cre/Cre}$ mice were ($rictor^{fl/+}$; $L7/Pcp\text{-}2^{Cre/Cre}$). Genotyping was performed by PCR on DNA isolated from toe using specific primers for the floxed region, the Cre transgenes, or the recombined alleles as described elsewhere (Bentzinger et al., 2008).

Tissue homogenization and Western blot analysis

Brains were dissected, transferred to protein lysate buffer (50 mM Tris-HCl, pH 7.5, 150 mM NaCl, 1 mM EDTA, 1% Triton X-100 supplemented with EDTA-free protease inhibitor cocktail tablets [Roche], and phosphatase inhibitor tablets PhosSTOP [Roche]), and homogenized with a glass/Teflon homogenizer using 10 strokes at 800 rpm. The homogenate was centrifuged at 13,600 *g* for 15 min at 4°C. Cleared lysates were then used to determine total protein amount (BCA Protein Assay; Thermo Fisher Scientific). After dilution with 4× SDS sample buffer, equal protein amounts were loaded onto SDS gels.

Antibodies

Rabbit polyclonal antibodies were as follows: P-PKCα (Ser657), PKCγ, and P-GAP-43 (Ser41) from Santa Cruz Biotechnology, Inc.; P-FoxO1 (Ser256), P-mTOR (Ser2448), P-mTOR (Ser2481), Akt, P-Akt (Thr308), P-GSK-3β (Ser9), mTOR, PKCα, S6 ribosomal protein, P-S6 ribosomal protein (Ser235/236), P-S6 kinase(Thr389), S6K, NDRG1, P-NDRG1 (Thr346), P-4E-BP (Thr37/46), P-eIF4E (Ser209), cleaved caspase3, P-MARCKS (Ser152/156), and PKCζ from Cell Signaling Technology; and P-PKCβ2 (Thr641) and P-PKCε (Ser729) from Abcam. Rabbit monoclonal antibodies were as follows: PKCε, β-actin, P-Akt (Ser473), GSK-3β, P-Tuberin (Thr1462), and Rictor from Cell Signaling Technology; and PKCβ2 from Abcam. Mouse monoclonal antibodies were as follows: β-tubulin from BD, Calbindin D-28K from Swant, GAP-43 from Invitrogen, NeuN from EMD Millipore, and MARCKS from Abcam. Guinea pig polyclonal antibodies were as follows: vGLUT1 and vGLUT2 from Synaptic Systems. Rat monoclonal antibodies were as follows: anti-BrdU from AbD Serotec.

Histology and immunohistochemistry

Mice were anesthetized with a lethal dose of Pentobarbital (300 mg/kg) and transcardially perfused with 4% PFA. Brains were removed and tissue processed with a Shandon Pathcenter and embedded in paraffin (Merck). Paraffin blocks were cut with a microtome into 3–5-µm-thick sagittal or coronal sections. Antigen retrieval was performed before immunostaining by boiling the sections in sodium citrate buffer (10 mM sodium citrate and 0.05% Tween 20, pH 6) for 20 min. Sections were rinsed twice in PBS, blocked with blocking buffer (5% BSA in PBS, and 0.2% Triton X-100) for 30 min, and incubated with primary antibody overnight at 4°C. Samples were washed three times with PBS and then stained with appropriate fluorescently labeled, secondary antibodies for 1 h at room temperature. Samples were mounted with Kaiser's glycerol gelatin (Merck). General histology on sections was performed using cresyl violet. Immunohistochemically stained sections were examined with a fluorescence microscope (model DM5000B; Leica) and a 10× objective (HC PL Apo, NA 0.4; Leica), a 20× objective (PL Fluotar, NA 0.5; Leica), a 40× objective (HCX Plan APO, NA 0.75; Leica), or a 63× objective (HCX PL APO, NA 1.32; Leica). Pictures were captured with a digital camera (F-View; Soft Imaging System) and analySIS software (Soft Imaging System). In some experiments, sections were imaged with the SPE confocal laser scanning microscope (model DMI4000B; Leica) using an ACS APO 40× objective (NA 1.15) or an ACS APO 63× objective (NA 1.3) at a resolution of 1024 × 1024 pixels. Pictures were captured using the built-in digital camera and software. Image analysis was performed using Imaris (Bitplane AG) or Adobe Photoshop CS5.

Golgi staining was performed by incubating freshly perfused mouse brains in Golgi solution (5% potassium dichromate, 5% potassium chromate,

Published April 8, 2013

and 5% mercuric chloride dissolved in H_2O) for 6 wk. The solution was changed every 2–3 days. Brains were subsequently dehydrated in 50, 70, 90, and 100% ethanol, each step for several days and then transferred to 2, 4, and 8% Celloidin solution. For embedding, 8% Celloidin was evaporated to 16%, hardened to a block, and cut with a vibratome into 200-µm sagittal sections. The sections were transferred onto gelatinized slides and stained first in ammonium hydroxide (14%) for 30 min followed by Kodak fix solution for 30 min. The sections were then dehydrated in 50, 70, 90, and 100% ethanol followed by 15 min in CXA solution (1:1:1 chloroform/xylol/ethanol) and embedded with Merckoglas (Merck). Microscopy was performed with a light microscope (model DM RB, Leica) using bright-field optics and 10, 20, or 40× objectives (PL Fluotar, NA 0.3–0.7; Leica). Pictures were captured with a digital camera (model DFC 420; Leica) and the appropriate software.

Quantification

Quantification of cell numbers used the method of isotropic fractionation as described elsewhere (Herculano-Houzel and Lent, 2005). In brief, brains were fixed for 3–30 d in 4% PFA and then mechanically dissociated with a glass/Teflon homogenizer in 40 mM sodium citrate and 1% Triton X-100. The homogenate was centrifuged for 10 min at 4,000 *g* and the supernatant was carefully removed. The pellet containing the nuclei was resuspended in 10 ml PBS containing 1% Hoechst dye. After sufficient agitation to achieve isotropy, 5-µl aliquots were removed and the number of nuclei was counted in a hemocytometer using a fluorescence microscope. Quantification of Golgi-stained neurons was performed by Neurolucida reconstruction and analysis with Neurolucida software. Volumetric quantification of brain areas was performed on cresyl violet–stained, 25-µm coronal paraffin sections. The arbitrary area of microscopic pictures taken at 2.5× was analyzed with Analysis software. Analysis of cell density was performed on sagittal, NeuN-stained, 5-µm-thick paraffin sections in the retrosplenial and visual cortex. Sholl analysis of dissociated hippocampal neurons was performed with Analysis software by counting the number of neurite crossings starting from the soma in a defined distance of 25 µm up to 125 µm. Quantification of Western blot protein band intensity was performed with the ImageJ program (National Institutes of Health). Quantification of the mean dendrite diameter of Purkinje cells was performed in sagittal, calbindin-stained cerebellar sections by measuring the dendrite diameter within the primary dendrite from the soma up to the first node. Apoptotic cells were quantified by staining P7 cortical sections with antibodies to cleaved caspase3. Cells were distinguished from blood vessels by counterstaining with Hoechst and the number of caspase3-positive cells per 1,000 cells (identified by Hoechst staining) was determined.

Statistical analysis

Statistical significance was assessed with the Student's *t* test or one-way Anova. Differences were considered to be statistically significant if the P value was less than 0.05. Quantitative data are presented as means ± SEM as indicated in the figure legends.

Electrophysiology

Mice were deeply sedated with isoflurane. After decapitation, the brain was rapidly removed and immediately transferred into ice-cold, oxygenated (95% O_2, 5% CO_2), low calcium artificial cerebrospinal fluid (ACSF) containing 119 mM NaCl, 1 mM NaH_2PO_4, 2.5 mM KCl, 0.125 mM $CaCl_2$, 3.3 mM $MgCl_2$, 11 mM D-glucose, and 26.2 mM $NaHCO_3$. Cerebella were cut with a vibratome into 250-µm sagittal sections in low calcium ACSF. Slices were transferred to oxygenated ACSF containing 119 mM NaCl, 1 mM NaH_2PO_4, 2.5 mM KCl, 2.5 mM $CaCl_2$, 1.3 mM $MgCl_2$, 11 mM D-glucose, and 26.2 mM $NaHCO_3$, incubated for 30 min at 34°C, and subsequently retained for at least 30 min at room temperature in oxygenated ACSF before recording. Miniature events were recorded using an Axopatch Multiclamp 700B amplifier (Molecular Devices) and borosilicate glass pipettes (4–6 mΩ) filled with intracellular solution (135 mM $CsMeSO_4$, 8 mM NaCl, 10 mM Hepes, 0.5 mM EGTA, 4 mM Mg-ATP, 0.3 mM Na-GTP, and 5 mM lidocaine-*N*-ethylbromide). For mEPSC recording, the holding potential was set to −70 mV. For mIPSC recording, the holding potential was set to 0 mV. In both conditions, the postsynaptic current was recorded for 10 min in the presence of 0.5 µM tetrodotoxin (TTX). Traces were further analyzed with the Mini Analysis Program v6 (Synaptosoft).

Biocytin labeling of single Purkinje cells

Biocytin was dissolved in the intracellular solution at a concentration of 3 mg/ml by sonication at 4°C. The orientation of the acute slice was noted for the whole-cell recordings. Staining procedure was adapted from Wierenga et al. (2008). In brief, after the recording, slices were fixed overnight at 4°C in 4% PFA dissolved in PBS. After extensive washing in PBS, slices were permeabilized and blocked for 24 h at 4°C in blocking solution (10% FBS in PBS, containing 0.4% Triton X-100) on a shaker. Anti-PKC-γ antibody was applied overnight at 4°C in blocking solution (5% FBS in PBS, containing 0.4% Triton X-100) on a shaker. After extensive washing with PBS, appropriate secondary antibodies were applied. Acute slices were mounted in Kaiser's glycerol gelatin with the patched side facing up. Stained slices were analyzed by confocal microscopy as described above using the 40× objective.

Single-cell RT-PCR

Purkinje cells were cell patch-clamped for 10–20 min using silanized patch pipettes filled with 7 µl of intracellular solution that contained biocytin as described above. After whole-cell recording, cytosol was harvested by aspiration and expelled into a PCR tube containing rRNasin (Promega), random hexamer primers, and dNTP (final concentrations are indicated below). The mixture was incubated for 5 min at 65°C and then chilled on ice before adding further components. mRNA was reverse transcribed in a 20-µl reaction volume containing 100 ng random hexamer primers, 0.5 mM dNTPs, 40 U rRNasin, 5 mM dithiothreitol, and 10 U SuperScript III reverse transcription (Invitrogen) in 1× "first strand buffer" (5× buffer: 0.25 M Tris-HCl, pH 8.3 at 25°C, 375 mM KCl, and 15 mM $MgCl_2$). The reaction mixture was incubated for 45 min at 50°C, followed by inactivation at 70°C for 15 min. 2 µl of the stopped reaction mixture were used as input cDNA for the subsequent nested two-step PCR, which was performed with the primer pairs P3–P4 for the first and P1–P2 for the second PCR, respectively. 35 cycles were performed for each PCR. The primer sequences are P1: 5′-GCCAAATTGCAAGGAGTATCA-3′; P2: 5′-TGAGTTGGCCACAGAACTAGG-3′; P3: 5′-CTGACCCGAGAACCTTCTGA-3′; P4: 5′-TTCCTGAAGCCCATCATTTC-3′. The primer pair P1–P2 results in an amplicon of 365 bp or 172 bp in case of the wild-type or the recombined allele, respectively.

Tissue cultures

Neurospheres were isolated from newborn (P0) mice. Pups were decapitated, and brains were removed and transferred into ice-cold Hank's buffered salt solution (HBSS; Invitrogen). Meninges were carefully removed under the dissection microscope and one brain half was transferred into freshly prepared neurosphere medium (NM) consisting of DMEM-F12 (1:1), supplemented with 1% penicillin/streptomycin, 0.2 mg/ml glutamine, 2% B27, 2 µg/ml heparin, 20 ng/ml EGF, and 10 ng/ml FGF2. The brain was carefully homogenized and plated on a 6-cm dish containing 4 ml NM and maintained in an incubator (36.5°C, 5% CO_2). After 4–5 d the neurospheres were trypinized, dissociated into single cell suspension, and the resulting secondary neurospheres were cultured for 6 d. 24 h before fixation, 10 µM BrdU was added to the medium. Neurospheres were fixed with 4% PFA and imaged at low magnification to determine the diameter of the neurospheres. To assess the number of the BrdU-positive cells, neurospheres were embedded in cryoprotective material, cut into 12-µm-thick sections, and immunostained with antibodies to BrdU. The number of BrdU-positive cells per sphere was counted and normalized to the sphere diameter.

Organotypic cerebellar slices were cultured as described elsewhere (Boukhtouche et al., 2006). In brief, P0 brains were dissected and transferred into ice-cold Gey's balanced salt solution. Meninges were carefully removed and cerebella dissected. With a tissue chopper (McIlwain), 350-µm-thick sagittal slices were cut and transferred into fresh Gey's solution. Slices were cultured on 0.4-µm membranes in 1 ml culture medium (50% basal medium with Earl's salts, 25% HBSS, 25% horse serum, 1 mM glutamine, and 5 mg/ml glucose) for 14 d. Culture medium was changed every 2–3 d.

Cultures of dissociated hippocampal neurons were prepared as follows: brains of P0 mice were dissected and transferred into ice-cold HBSS. Hippocampi were removed, trypsinized for 15 min, and dissociated. Cells were plated onto poly-L-lysine–coated coverslips at a density of 90,000 cells per well in a 24-well plate. Neurons were grown for 14 d. After 7 d, neurons were transfected with constructs encoding GFP under the synapsin promoter using Lipofectamine. After 14 d, cultures were fixed with 4% PFA in PBS containing 120 mM sucrose, washed in PBS, and embedded with Kaiser's glycerol gelatin.

Mouse behavior

For hindlimb clasping assessment, 1-yr-old mice were lifted by the tail and held over the cage for up to 2 min. Clasping was scored when mice crossed hindlimbs for more than 3 s. The rotarod test was performed by placing 10-wk-old mice on a rod that accelerated from 5 rpm to 30 rpm in 2 min. Latency to fall off the rod was measured.

Published April 8, 2013

Online supplemental material

Fig. S1 shows that the number of apoptotic cells as visualized by caspase3 staining is not increased and that cell density of NeuN-positive neurons is increased in RibKO mice. Fig. S2 shows that phosphorylation of PKCα, PKCβ2, and PKCε is greatly reduced in RibKO mice. Fig. S3 shows that PKCγ-negative Purkinje cells in RiPuKO mice are deficient for rictor. Online supplemental material is available at http://www.jcb.org/cgi/content/full/jcb.201205030/DC1.

We thank M. Gassmann and J. Kapfhammer for reading the manuscript; S. Frank for his help in the initial analysis of the histology; members of the laboratory of M. Hall for reagents and discussions; F. Boukhtouche for the help in setting up cerebellar slice cultures; and P. Scheiffele for providing us with the *L7/Pcp-2-Cre* mice.

This work was supported by the Swiss National Science Foundation, the Cantons of Basel-Stadt and Basel-Landschaft, and Swiss Life.

Submitted: 4 May 2012
Accepted: 12 March 2013

References

Benowitz, L.I., and A. Routtenberg. 1997. GAP-43: an intrinsic determinant of neuronal development and plasticity. *Trends Neurosci.* 20:84–91. http://dx.doi.org/10.1016/S0166-2236(96)10072-2

Bentzinger, C.F., K. Romanino, D. Cloëtta, S. Lin, J.B. Mascarenhas, F. Oliveri, J. Xia, E. Casanova, C.F. Costa, M. Brink, et al. 2008. Skeletal muscle-specific ablation of raptor, but not of rictor, causes metabolic changes and results in muscle dystrophy. *Cell Metab.* 8:411–424. http://dx.doi.org/10.1016/j.cmet.2008.10.002

Boukhtouche, F., S. Janmaat, G. Vodjdani, V. Gautheron, J. Mallet, I. Dusart, and J. Mariani. 2006. Retinoid-related orphan receptor alpha controls the early steps of Purkinje cell dendritic differentiation. *J. Neurosci.* 26:1531–1538. http://dx.doi.org/10.1523/JNEUROSCI.4636-05.2006

Calabrese, B., and S. Halpain. 2005. Essential role for the PKC target MARCKS in maintaining dendritic spine morphology. *Neuron*. 48:77–90. http://dx.doi.org/10.1016/j.neuron.2005.08.027

Chen, D.H., Z. Brkanac, C.L. Verlinde, X.J. Tan, L. Bylenok, D. Nochlin, M. Matsushita, H. Lipe, J. Wolff, M. Fernandez, et al. 2003. Missense mutations in the regulatory domain of PKC gamma: a new mechanism for dominant nonepisodic cerebellar ataxia. *Am. J. Hum. Genet.* 72:839–849. http://dx.doi.org/10.1086/373883

Cole, E.H., O. Johnston, C.L. Rose, and J.S. Gill. 2008. Impact of acute rejection and new-onset diabetes on long-term transplant graft and patient survival. *Clin. J. Am. Soc. Nephrol.* 3:814–821. http://dx.doi.org/10.2215/CJN.04681107

Crino, P.B. 2011. mTOR: A pathogenic signaling pathway in developmental brain malformations. *Trends Mol. Med.* 17:734–742. http://dx.doi.org/10.1016/j.molmed.2011.07.008

Cybulski, N., P. Polak, J. Auwerx, M.A. Rüegg, and M.N. Hall. 2009. mTOR complex 2 in adipose tissue negatively controls whole-body growth. *Proc. Natl. Acad. Sci. USA*. 106:9902–9907. http://dx.doi.org/10.1073/pnas.0811321106

Easton, R.M., H. Cho, K. Roovers, D.W. Shineman, M. Mizrahi, M.S. Forman, V.M. Lee, M. Szabolcs, R. de Jong, T. Oltersdorf, et al. 2005. Role for Akt3/protein kinase Bgamma in attainment of normal brain size. *Mol. Cell. Biol.* 25:1869–1878. http://dx.doi.org/10.1128/MCB.25.5.1869-1878.2005

Ehninger, D., and A.J. Silva. 2011. Rapamycin for treating Tuberous sclerosis and Autism spectrum disorders. *Trends Mol. Med.* 17:78–87. http://dx.doi.org/10.1016/j.molmed.2010.10.002

Facchinetti, V., W. Ouyang, H. Wei, N. Soto, A. Lazorchak, C. Gould, C. Lowry, A.C. Newton, Y. Mao, R.Q. Miao, et al. 2008. The mammalian target of rapamycin complex 2 controls folding and stability of Akt and protein kinase C. *EMBO J.* 27:1932–1943. http://dx.doi.org/10.1038/emboj.2008.120

Fremeau, R.T. Jr., M.D. Troyer, I. Pahner, G.O. Nygaard, C.H. Tran, R.J. Reimer, E.E. Bellocchio, D. Fortin, J. Storm-Mathisen, and R.H. Edwards. 2001. The expression of vesicular glutamate transporters defines two classes of excitatory synapse. *Neuron*. 31:247–260. http://dx.doi.org/10.1016/S0896-6273(01)00344-0

García-Martínez, J.M., and D.R. Alessi. 2008. mTOR complex 2 (mTORC2) controls hydrophobic motif phosphorylation and activation of serum- and glucocorticoid-induced protein kinase 1 (SGK1). *Biochem. J.* 416:375–385. http://dx.doi.org/10.1042/BJ20081668

Gödel, M., B. Hartleben, N. Herbach, S. Liu, S. Zschiedrich, S. Lu, A. Debreczeni-Mór, M.T. Lindenmeyer, M.P. Rastaldi, G. Hartleben, et al. 2011. Role of mTOR in podocyte function and diabetic nephropathy in humans and mice. *J. Clin. Invest.* 121:2197–2209. http://dx.doi.org/10.1172/JCI44774

Graus-Porta, D., S. Blaess, M. Senften, A. Littlewood-Evans, C. Damsky, Z. Huang, P. Orban, R. Klein, J.C. Schittny, and U. Müller. 2001. Beta1-class integrins regulate the development of laminae and folia in the cerebral and cerebellar cortex. *Neuron*. 31:367–379. http://dx.doi.org/10.1016/S0896-6273(01)00374-9

Guertin, D.A., D.M. Stevens, C.C. Thoreen, A.A. Burds, N.Y. Kalaany, J. Moffat, M. Brown, K.J. Fitzgerald, and D.M. Sabatini. 2006. Ablation in mice of the mTORC components raptor, rictor, or mLST8 reveals that mTORC2 is required for signaling to Akt-FOXO and PKCalpha, but not S6K1. *Dev. Cell*. 11:859–871. http://dx.doi.org/10.1016/j.devcel.2006.10.007

Guertin, D.A., D.M. Stevens, M. Saitoh, S. Kinkel, K. Crosby, J.H. Sheen, D.J. Mullholland, M.A. Magnuson, H. Wu, and D.M. Sabatini. 2009. mTOR complex 2 is required for the development of prostate cancer induced by Pten loss in mice. *Cancer Cell*. 15:148–159. http://dx.doi.org/10.1016/j.ccr.2008.12.017

Herculano-Houzel, S., and R. Lent. 2005. Isotropic fractionator: a simple, rapid method for the quantification of total cell and neuron numbers in the brain. *J. Neurosci.* 25:2518–2521. http://dx.doi.org/10.1523/JNEUROSCI.4526-04.2005

Hietakangas, V., and S.M. Cohen. 2007. Re-evaluating AKT regulation: role of TOR complex 2 in tissue growth. *Genes Dev.* 21:632–637. http://dx.doi.org/10.1101/gad.416307

Hisano, S., K. Sawada, M. Kawano, M. Kanemoto, G. Xiong, K. Mogi, H. Sakata-Haga, J. Takeda, Y. Fukui, and H. Nogami. 2002. Expression of inorganic phosphate/vesicular glutamate transporters (BNPI/VGLUT1 and DNPI/VGLUT2) in the cerebellum and precerebellar nuclei of the rat. *Brain Res. Mol. Brain Res.* 107:23–31. http://dx.doi.org/10.1016/S0169-328X(02)00442-4

Ikenoue, T., K. Inoki, Q. Yang, X. Zhou, and K.L. Guan. 2008. Essential function of TORC2 in PKC and Akt turn motif phosphorylation, maturation and signalling. *EMBO J.* 27:1919–1931. http://dx.doi.org/10.1038/emboj.2008.119

Jacinto, E., R. Loewith, A. Schmidt, S. Lin, M.A. Rüegg, A. Hall, and M.N. Hall. 2004. Mammalian TOR complex 2 controls the actin cytoskeleton and is rapamycin insensitive. *Nat. Cell Biol.* 6:1122–1128. http://dx.doi.org/10.1038/ncb1183

Kapfhammer, J.P. 2004. Cellular and molecular control of dendritic growth and development of cerebellar Purkinje cells. *Prog. Histochem. Cytochem.* 39:131–182. http://dx.doi.org/10.1016/j.proghi.2004.07.002

Kim, D.H., D.D. Sarbassov, S.M. Ali, J.E. King, R.R. Latek, H. Erdjument-Bromage, P. Tempst, and D.M. Sabatini. 2002. mTOR interacts with raptor to form a nutrient-sensitive complex that signals to the cell growth machinery. *Cell*. 110:163–175. http://dx.doi.org/10.1016/S0092-8674(02)00808-5

Kumar, A., T.E. Harris, S.R. Keller, K.M. Choi, M.A. Magnuson, and J.C. Lawrence Jr. 2008. Muscle-specific deletion of rictor impairs insulin-stimulated glucose transport and enhances Basal glycogen synthase activity. *Mol. Cell. Biol.* 28:61–70. http://dx.doi.org/10.1128/MCB.01405-07

Lamming, D.W., L. Ye, P. Katajisto, M.D. Goncalves, M. Saitoh, D.M. Stevens, J.G. Davis, A.B. Salmon, A. Richardson, R.S. Ahima, et al. 2012. Rapamycin-induced insulin resistance is mediated by mTORC2 loss and uncoupled from longevity. *Science*. 335:1638–1643. http://dx.doi.org/10.1126/science.1215135

Laplante, M., and D.M. Sabatini. 2012. mTOR signaling in growth control and disease. *Cell*. 149:274–293. http://dx.doi.org/10.1016/j.cell.2012.03.017

Larsell, O. 1952. The morphogenesis and adult pattern of the lobules and fissures of the cerebellum of the white rat. *J. Comp. Neurol.* 97:281–356. http://dx.doi.org/10.1002/cne.900970204

Lein, E.S., M.J. Hawrylycz, N. Ao, M. Ayres, A. Bensinger, A. Bernard, A.F. Boe, M.S. Boguski, K.S. Brockway, E.J. Byrnes, et al. 2007. Genome-wide atlas of gene expression in the adult mouse brain. *Nature*. 445:168–176. http://dx.doi.org/10.1038/nature05453

Li, H., G. Chen, B. Zhou, and S. Duan. 2008. Actin filament assembly by myristoylated alanine-rich C kinase substrate-phosphatidylinositol-4, 5-diphosphate signaling is critical for dendrite branching. *Mol. Biol. Cell*. 19:4804–4813. http://dx.doi.org/10.1091/mbc.E08-03-0294

Loewith, R., E. Jacinto, S. Wullschleger, A. Lorberg, J.L. Crespo, D. Bonenfant, W. Oppliger, P. Jenoe, and M.N. Hall. 2002. Two TOR complexes, only one of which is rapamycin sensitive, have distinct roles in cell growth control. *Mol. Cell*. 10:457–468. http://dx.doi.org/10.1016/S1097-2765(02)00636-6

Mazei-Robison, M.S., J.W. Koo, A.K. Friedman, C.S. Lansink, A.J. Robison, M. Vinish, V. Krishnan, S. Kim, M.A. Siuta, A. Galli, et al. 2011. Role for mTOR signaling and neuronal activity in morphine-induced adaptations in ventral tegmental area dopamine neurons. *Neuron*. 72:977–990. http://dx.doi.org/10.1016/j.neuron.2011.10.012

Metzger, F. 2010. Molecular and cellular control of dendrite maturation during brain development. *Curr Mol Pharmacol*. 3:1–11.

Ohno, S., and Y. Nishizuka. 2002. Protein kinase C isotypes and their specific functions: prologue. *J. Biochem.* 132:509–511. http://dx.doi.org/10.1093/oxfordjournals.jbchem.a003249

Polak, P., N. Cybulski, J.N. Feige, J. Auwerx, M.A. Rüegg, and M.N. Hall. 2008. Adipose-specific knockout of raptor results in lean mice with enhanced mitochondrial respiration. *Cell Metab.* 8:399–410. http://dx.doi.org/10.1016/j.cmet.2008.09.003

Read, D.E., and A.M. Gorman. 2009. Involvement of Akt in neurite outgrowth. *Cell. Mol. Life Sci.* 66:2975–2984. http://dx.doi.org/10.1007/s00018-009-0057-8

Richter, J.D., and E. Klann. 2009. Making synaptic plasticity and memory last: mechanisms of translational regulation. *Genes Dev*. 23:1–11. http://dx.doi.org/10.1101/gad.1735809

Risson, V., L. Mazelin, M. Roceri, H. Sanchez, V. Moncollin, C. Corneloup, H. Richard-Bulteau, A. Vignaud, D. Baas, A. Defour, et al. 2009. Muscle inactivation of mTOR causes metabolic and dystrophin defects leading to severe myopathy. *J. Cell Biol.* 187:859–874. http://dx.doi.org/10.1083/jcb.200903131

Russell, R.C., C. Fang, and K.L. Guan. 2011. An emerging role for TOR signaling in mammalian tissue and stem cell physiology. *Development*. 138:3343–3356. http://dx.doi.org/10.1242/dev.058230

Saito, H., H. Tsumura, S. Otake, A. Nishida, T. Furukawa, and N. Suzuki. 2005. L7/Pcp-2-specific expression of Cre recombinase using knock-in approach. *Biochem. Biophys. Res. Commun.* 331:1216–1221. http://dx.doi.org/10.1016/j.bbrc.2005.04.043

Sarbassov, D.D., S.M. Ali, D.H. Kim, D.A. Guertin, R.R. Latek, H. Erdjument-Bromage, P. Tempst, and D.M. Sabatini. 2004. Rictor, a novel binding partner of mTOR, defines a rapamycin-insensitive and raptor-independent pathway that regulates the cytoskeleton. *Curr. Biol.* 14:1296–1302. http://dx.doi.org/10.1016/j.cub.2004.06.054

Sarbassov, D.D., D.A. Guertin, S.M. Ali, and D.M. Sabatini. 2005. Phosphorylation and regulation of Akt/PKB by the rictor-mTOR complex. *Science*. 307:1098–1101. http://dx.doi.org/10.1126/science.1106148

Sarbassov, D.D., S.M. Ali, S. Sengupta, J.H. Sheen, P.P. Hsu, A.F. Bagley, A.L. Markhard, and D.M. Sabatini. 2006. Prolonged rapamycin treatment inhibits mTORC2 assembly and Akt/PKB. *Mol. Cell*. 22:159–168. http://dx.doi.org/10.1016/j.molcel.2006.03.029

Seki, T., N. Adachi, N. Abe-Seki, T. Shimahara, H. Takahashi, K. Yamamoto, N. Saito, and N. Sakai. 2011. Elucidation of the molecular mechanism and exploration of novel therapeutics for spinocerebellar ataxia caused by mutant protein kinase Cγ. *J. Pharmacol. Sci.* 116:239–247. http://dx.doi.org/10.1254/jphs.11R04CP

Shiota, C., J.T. Woo, J. Lindner, K.D. Shelton, and M.A. Magnuson. 2006. Multiallelic disruption of the rictor gene in mice reveals that mTOR complex 2 is essential for fetal growth and viability. *Dev. Cell*. 11:583–589. http://dx.doi.org/10.1016/j.devcel.2006.08.013

Sidman, R.L., P.W. Lane, and M.M. Dickie. 1962. Staggerer, a new mutation in the mouse affecting the cerebellum. *Science*. 137:610–612. http://dx.doi.org/10.1126/science.137.3530.610

Sillitoe, R.V., and A.L. Joyner. 2007. Morphology, molecular codes, and circuitry produce the three-dimensional complexity of the cerebellum. *Annu. Rev. Cell Dev. Biol.* 23:549–577. http://dx.doi.org/10.1146/annurev.cellbio.23.090506.123237

Siuta, M.A., S.D. Robertson, H. Kocalis, C. Saunders, P.J. Gresch, V. Khatri, C. Shiota, J.P. Kennedy, C.W. Lindsley, L.C. Daws, et al. 2010. Dysregulation of the norepinephrine transporter sustains cortical hypodopaminergia and schizophrenia-like behaviors in neuronal rictor null mice. *PLoS Biol.* 8:e1000393. http://dx.doi.org/10.1371/journal.pbio.1000393

Sucher, N.J., D.L. Deitcher, D.J. Baro, R.M. Warrick, and E. Guenther. 2000. Genes and channels: patch/voltage-clamp analysis and single-cell RT-PCR. *Cell Tissue Res.* 302:295–307. http://dx.doi.org/10.1007/s004410000289

Tronche, F., C. Kellendonk, O. Kretz, P. Gass, K. Anlag, P.C. Orban, R. Bock, R. Klein, and G. Schütz. 1999. Disruption of the glucocorticoid receptor gene in the nervous system results in reduced anxiety. *Nat. Genet.* 23:99–103. http://dx.doi.org/10.1038/12703

Tschopp, O., Z.Z. Yang, D. Brodbeck, B.A. Dummler, M. Hemmings-Mieszczak, T. Watanabe, T. Michaelis, J. Frahm, and B.A. Hemmings. 2005. Essential role of protein kinase B gamma (PKB gamma/Akt3) in postnatal brain development but not in glucose homeostasis. *Development*. 132:2943–2954. http://dx.doi.org/10.1242/dev.01864

Wetts, R., and K. Herrup. 1982. Interaction of granule, Purkinje and inferior olivary neurons in lurcher chimeric mice. II. Granule cell death. *Brain Res.* 250:358–362. http://dx.doi.org/10.1016/0006-8993(82)90431-0

Wierenga, C.J., N. Becker, and T. Bonhoeffer. 2008. GABAergic synapses are formed without the involvement of dendritic protrusions. *Nat. Neurosci.* 11:1044–1052. http://dx.doi.org/10.1038/nn.2180

Wullschleger, S., R. Loewith, and M.N. Hall. 2006. TOR signaling in growth and metabolism. *Cell*. 124:471–484. http://dx.doi.org/10.1016/j.cell.2006.01.016